ACS MATERIALS LETTERS

www.acsmaterialsletters.org

REVIEW

Multispectral Thermal Management Designs for Net-Zero Energy Buildings

Xiuqiang Li, Wanrong Xie, Chenxi Sui, and Po-Chun Hsu*

Cite This: *ACS Materials Lett.* 2020, 2, 1624–1643

Read Online

ACCESS | Metrics & More | Article Recommendations

ABSTRACT: The energy consumption of building for heating and cooling accounts for about 15% of the total energy consumption of the world. Owing to the rapid progress in nanophotonic materials, innovative technologies based on multispectral design and tuning have obtained significant development and provided new opportunities to decrease the energy consumption of buildings. Based on this background, this review aims to summarize state-of-the-art progress of daytime radiative cooling, smart windows, and personal thermal management toward net-zero energy buildings based on multispectral material and photonic engineering. Unsolved scientific and technical challenges associated with future perspectives in this field are also discussed, hoping to promote the development of building energy-saving technologies for our sustainable future.

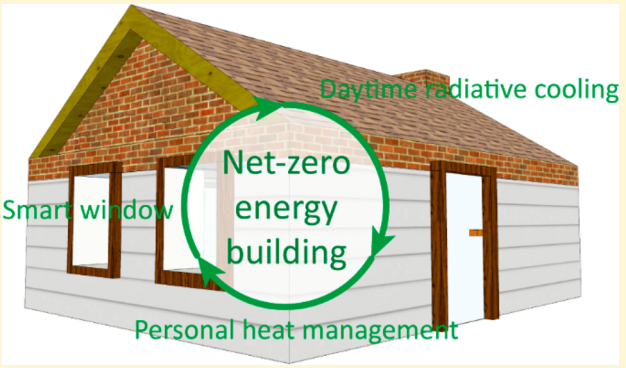

Currently, buildings are responsible for over 30% of total global energy consumption and 10% of global greenhouse gas emissions.[1] Among this huge energy consumption, approximately half is for heat management, including heating and cooling. It is predicted that energy consumption for building temperature control will grow by 80% over the period 2010−2050 due to climate change and population growth.[2] Therefore, how to develop innovative and sustainable technologies to mitigate the building energy consumption with a minimal carbon footprint—known as "net-zero energy buildings"—has become a vital issue for both science and industry communities.

The ultimate goal of net-zero energy building is, as the name suggests, to completely eliminate the energy demand for the fossil-fuel-dominated electricity grid by utilizing renewable energy in a highly efficient manner. For building space heating, the well-known approach is to use the sun and directly convert solar radiation into thermal energy. In thermodynamic and photonic terms, this requires the absorption of the black body radiation at 5778 K that peaks at 550 nm and spans visible ($400\ \text{nm} \le \lambda < 700\ \text{nm}$) and near-infrared (near-IR, $700\ \text{nm} \le \lambda < 4000\ \text{nm}$). For building space cooling, a promising emerging solution is daytime radiative cooling, which aims to reflect all of the solar radiation and let the buildings (~300 K) directly emit room temperature black body radiation toward the deep space (3 K). This radiation peaks at approximately 10 μm and covers the middle-infrared region (mid-IR, $4000\ \text{nm} \le \lambda < 40000\ \text{nm}$). To extend the discussion from pure heat transfer to building−human interaction, one can further realize that visible light and near-IR also have drastically different applications and require separate controls—the former contains vision, color, and heat, and the latter is only for heat. Ideal thermal management methods for net-zero buildings should be equipped with all tuning capabilities (transmittance, reflection, and absorption/emission) in all three wavelength ranges (visible, near-IR, and mid-IR) to make the best use of renewable energy (Figure 1a and b).[3−8] Note that absorption and emission are equivalent at the thermodynamic equilibrium, according to Kirchhoff's radiation law. In other words, for the electromagnetic wave of the same wavelength, objects that are absorptive must also be emissive.

Figure 1b presents the general design guideline for the ones who aspire to boost the heating/cooling performance using multispectrally engineered materials. For example, to accomplish the best heating performance for building roofs/walls, the materials should be absorptive in both visible and near-IR but reflective in mid-IR. These multispectral thermal management designs require cross-disciplinary efforts from thermal engi-

Received: July 16, 2020
Accepted: October 27, 2020
Published: November 10, 2020

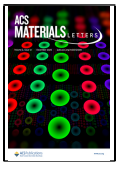

https://dx.doi.org/10.1021/acsmaterialslett.0c00322
ACS Materials Lett. 2020, 2, 1624−1643

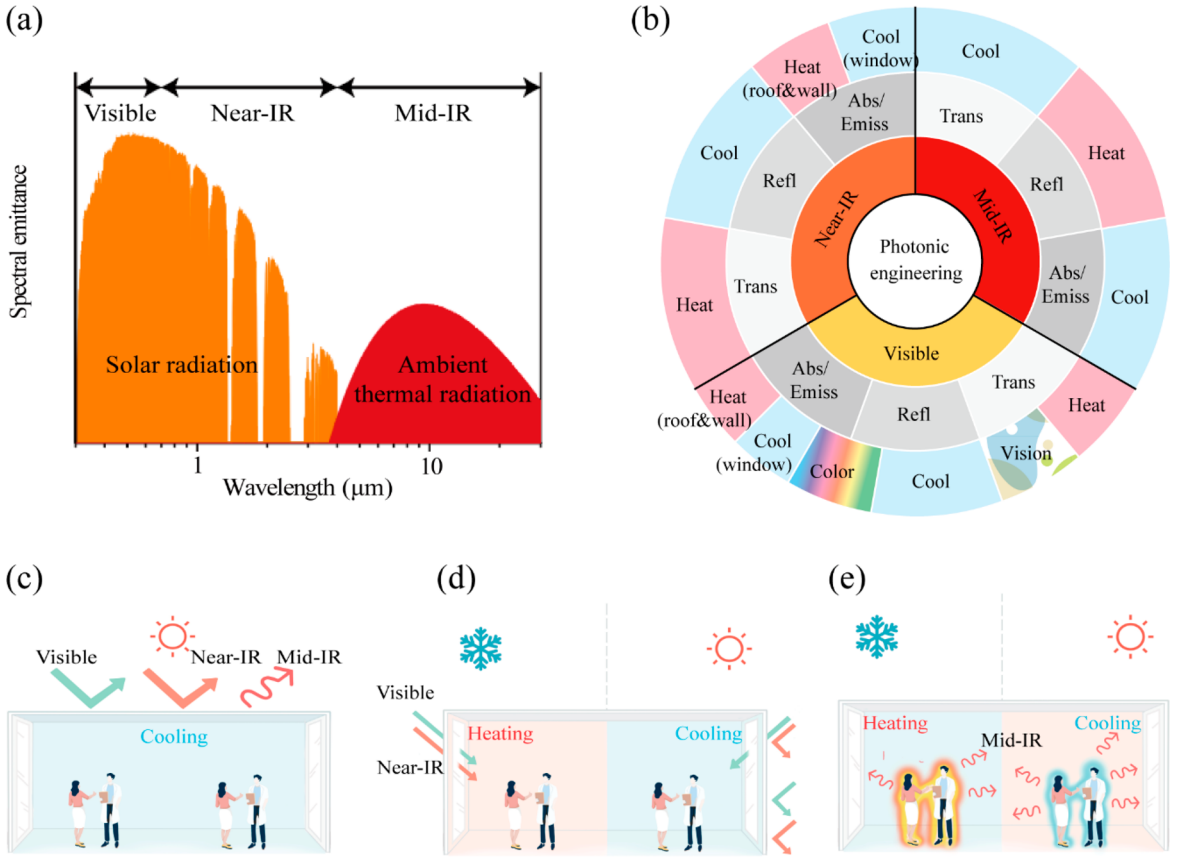

Figure 1. Multispectral designs for building energy efficiency. (a) The spectra of solar radiation and ambient thermal radiation, which includes visible, near-IR, and mid-IR. (b) The hierarchical pie graph that summarizes the multispectral photonic engineering for net-zero energy buildings. From the core to the shell, the graph encompasses types of radiation, tunable properties, and the effects on the subjects (buildings and/or residents). (c) Working principle of daytime radiative cooling, (d) smart windows, and (e) personal thermal management cloth.

neering, photonics design, materials science, and system integration. For example, (1) daytime radiative cooling is achieved by reflecting the major part of solar energy (0−2.5 μm) and emitting mid-IR thermal radiation to the deep space (3K) through the atmospheric transparent window between 8 and 13 μm, as illustrated in Figures 1c and 2b. Sub-ambient cooling can be achieved with proper thermal insulation[3,4] and result in significant energy savings. A prior study suggests that for a medium commercial building (3330 m^2 floor area) defined by the US Department of Energy located in Las Vegas where 60% of the roof is assumed to be covered by the radiative cooling panels, electricity consumption for cooling during the summer could be reduced by 21%.[5] (2) Smart windows realize energy saving by regulating visible and near-IR (see Figure 1d), which constitute 50 and 43% of the total solar energy. It is reported that, compared to the traditional low emissivity glass, the saving of overall building energy consumption can reach about 10% when the smart window is used.[6] (3) Personal thermal management cloth is also a promising strategy to reduce heating ventilation and air conditioning (HVAC) energy consumption by focusing on the local environment around the human body instead of the entire building interior space (see Figure 1e). Tuning the thermal radiation of cloth is an effective way to achieve personal thermal management. Generally, the ideal temperature range for the building is from 21.1 to 23.9 °C, which can be expanded about 2 °C on both hot and cold sides after using personal thermal management technologies, and corresponding energy saving can reach to approximately 15% of total building energy consumption.[7,8] Apart from the mid-IR consideration for energy saving, personal thermal management cloth also needs to consider the visible design due to the requirement of privacy and personal aesthetic preferences.

This paper summarizes state-of-the-art progress of daytime radiative cooling, smart windows, and personal thermal management toward net-zero energy buildings based on multispectral material and photonic engineering.

Motivated by its significance in both fundamental study and transformative engineering, this review aspires to highlight current multispectral design for building thermal management and provides insights for the broad community. Here, we will focus on technologies that have not yet been adopted on a large scale, such as daytime radiative cooling, smart window, and personal thermal management cloth. The basic principle, state-of-the-art progress, challenges, and perspectives of these technologies will be discussed.

https://dx.doi.org/10.1021/acsmaterialslett.0c00322
ACS Materials Lett. 2020, 2, 1624−1643

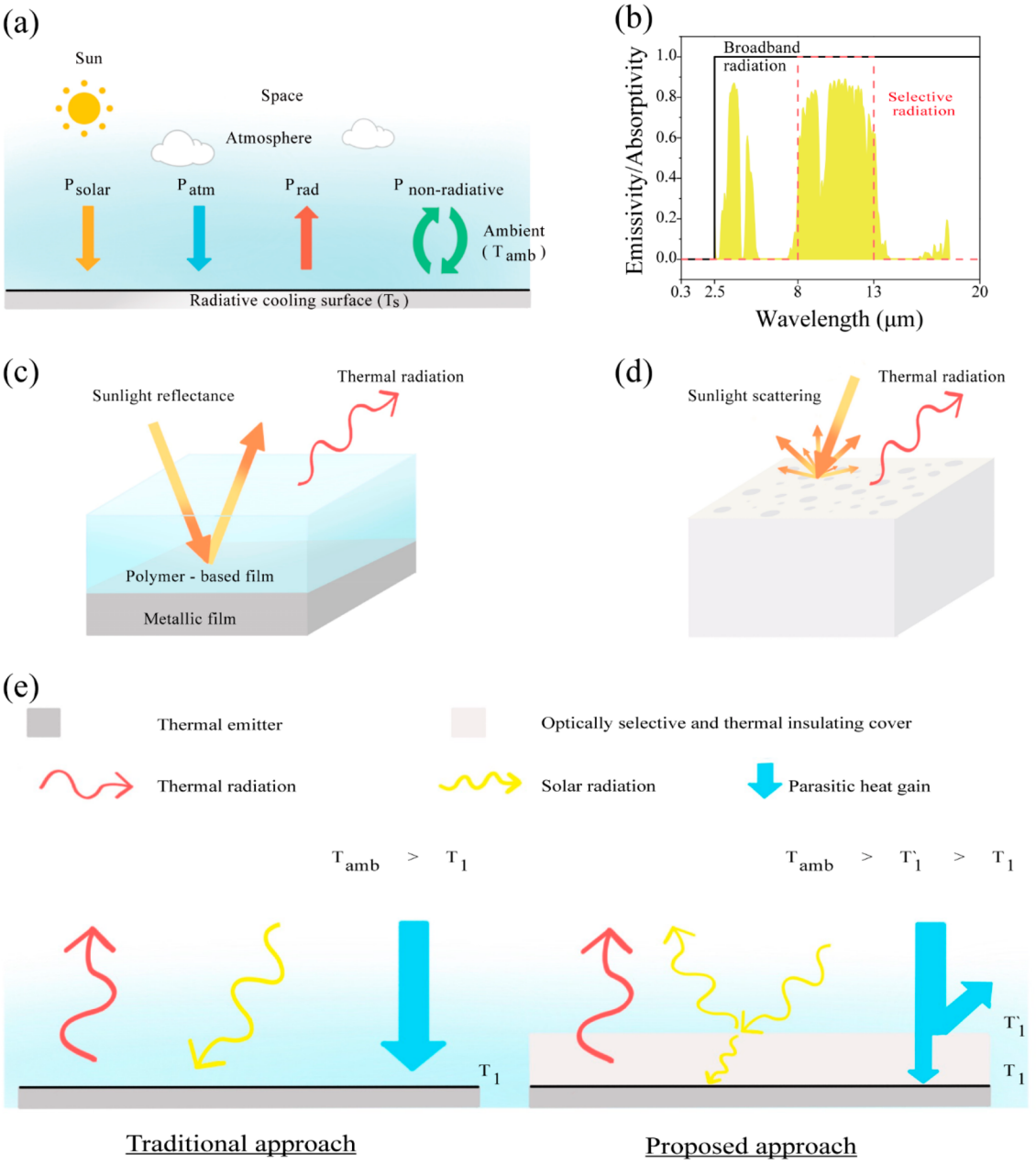

Figure 2. Daytime radiative cooling working principles and design concept. (a) Heat transfer processes on a radiative cooling surface. (b) Ideal emissivity spectrum of radiative cooling materials (the atmospheric transmittance window (yellow shaded area) is plotted for reference). (c) Radiative cooling materials based on metallic films to efficiently reflect the sunlight. (d) Radiative cooling materials based on multiscale pores, channels, and/or fibers to efficiently scatter the sunlight. (e) Traditional radiative cooling device (left) and radiative cooling device with PE aerogel (right).

■ DAYTIME RADIATIVE COOLING

Radiative cooling has a long history in building thermal engineering. However, it traditionally only considers the nighttime cooling that operates upon mid-IR emission through the atmospheric window.[4,9] Daytime radiative cooling, on the other hand, had been challenging to achieve because the radiation cooling energy (usually <150 W/m^2) can be easily offset by the strong solar energy.[4] In 2014, Raman et al.[3] first demonstrated the daytime radiative cooling below the ambient temperature in the daytime using an integrated photonic solar reflector and thermal emitter consisting of seven alternating HfO_2/SiO_2 layers that are optimized to reflect 97% of sunlight while emitting strongly in the atmospheric transparency window. In the past few years, significant progress has been made, making daytime radiative cooling an attractive method to supply cooling with zero energy consumption.[10−28]

■ THEORETICAL MODEL

In order to explain the potential influencing factors and to give a guideline to design for higher daytime cooling power, the numerical model for daytime radiative cooling is discussed below.[3,4] As shown in Figure 2a, the net cooling power (P_{net}) of a daytime radiative cooling device could be described as

$$P_{net} = P_{rad} - P_{atm} - P_{solar} - P_{non\text{-}rad} \quad (1)$$

https://dx.doi.org/10.1021/acsmaterialslett.0c00322
ACS Materials Lett. 2020, 2, 1624−1643

Table 1. Summarization of the Daytime Radiative Cooling Experimental Works

materials	material properties	cooling performance	reference
seven layers of alternating SiO_2 and HfO_2 thermal emitters backed by a silver solar reflector (200 nm)	solar reflectance: 0.97 mid-IR emittances: none given	achieving about 40.1 W/m^2 cooling power and a sub-ambient temperature drop of 4.9 °C	3
a visibly reflective extruded copolymer mirror (3M Vikiuiti ESR film), on top of an enhanced silver reflective surface	none given	panels cool water up to 5 °C below the ambient air temperature at water flow rates of 0.2 L/min m^2, corresponding to an effective heat rejection flux of up to 70 W/m^2	5
100 μm polydimethylsiloxane (PDMS)/500 μm fused silica wafer/120 nm silver film	none given	achieving sub-ambient temperature drops of 8.2 °C under direct sunlight and 8.4 °C at night	14
Vikuiti enhanced specular reflector film (3M) on 200 nm silver film	solar reflectance: 0.97 mid-IR emittances: 0.96	achieving 2 °C sub-ambient temperature drops under 1060 W/m^2 solar irradiance	15
randomized SiO_2 microparticles dispersed in polymethylpentene polymers on 200 nm silver film	solar reflectance: 0.96 mid-IR emittances: 0.93	the average cooling power reaches 93 W/m^2 under normal-incidence solar irradiance larger than 900 W/m^2	13, 23, 26
150 μm PDMS film on Al film	solar reflectance: 0.90 mid-IR emittances: 0.946	realizing continuous sub-ambient temperature drops of ∼2−9 °C on a typical clear sunny day	27
wood	solar reflectance: 0.96 mid-IR emittances: 0.90	achieving 63 and 16 W/m^2 cooling powers during the night and daytime (between 11 a.m. and 2 p.m.) and 53 W/m^2 average cooling power over the 24 h period	18
hierarchically porous poly(vinylidene fluoride-*co*-hexafluoropropene) (P(VdF-HFP)HP)	solar reflectance: 0.96 ± 0.03 emittances (8−13 μm): 0.97 ± 0.02	achieving sub-ambient temperature drops of ∼6 °C and cooling powers of ∼96 W/m^2 under solar intensities of 890 and 750 W/m^2, respectively	20

where P_{rad}, P_{atm}, P_{solar}, and $P_{non\text{-}rad}$ are the outward radiation power of the device itself, inward radiation power of the ambient, solar radiation, and non-radiative heat flux, respectively.

In the above equation, P_{rad}, P_{atm}, and P_{solar} are described based on Planck's blackbody radiation law below

$$P_{rad}(T_s) = \int \cos\theta \, d\Omega \int_0^\infty I_{bb}(\lambda, T_s)\varepsilon_s(\Omega, \lambda) \, d\lambda \quad (2)$$

$$P_{atm}(T_{amb}) = \int \cos\theta \, d\Omega \int_0^\infty I_{bb}(\lambda, T_{amb}) \varepsilon_s(\Omega, \lambda)\varepsilon_{atm}(\Omega, \lambda) \, d\lambda \quad (3)$$

$$P_{solar} = \cos\theta \int_0^\infty \varepsilon_s(\theta, \lambda) I_{solar}(\lambda) \, d\lambda \quad (4)$$

$\int d\Omega = \int_0^{\pi/2} d\theta \sin\theta \int_0^{2\pi} d\phi$ is the angular integral over a hemisphere. $I_{bb}(T, \lambda)$ is the blackbody radiance at a certain temperature and wavelength, which is calculated by $I_{bb} = \frac{2hc^2}{\lambda^5} \frac{1}{e^{hc/\lambda k_B T} - 1}$, where h is the Planck constant, k_B is the Boltzmann constant, c is the speed of light, and λ is the wavelength. In eq 2, T_s is the surface temperature of the cooling device. $\varepsilon_s(\Omega, \lambda)$ is the emissivity of the cooling material. This coefficient is the function of wavelength and incident angle. In eq 3, T_{amb} is the ambient temperature of the atmosphere. $\varepsilon_s(\Omega, \lambda)$ and $\varepsilon_{atm}(\Omega, \lambda)$ are the emissivity of the cooling material and atmosphere, respectively. $\varepsilon_{atm}(\Omega, \lambda)$ is determined by many factors, such as humidity, altitude, and cloud coverage. It is worth noting that this number of $\varepsilon_{atm}(\Omega, \lambda)$ can be directly obtained by ATRAN—a web-based software when the corresponding influencing factors are entered.[29] Similarly, in eq 3, $\varepsilon_s(\theta, \lambda)$ is the emissivity/absorptivity of the cooling material in the solar spectrum and $I_{solar}(\lambda)$ is the direct spectral solar irradiance. The last term, $P_{non\text{-}rad}$, is contributed by convection and conduction

$$P_{non\text{-}rad} = h(T_{amb} - T_s) \quad (5)$$

where h is the overall heat transfer coefficient, written as $h = h_{conv} + h_{cond}$, where h_{cond} and h_{cond} are the heat transfer coefficients of convection and conduction.

According to the equations above, if we want to obtain a large daytime radiative cooling power, it should maximize P_{rad} and suppress P_{atm}, P_{solar}, and $P_{non\text{-}rad}$. P_{atm} is mainly determined by the weather conditions.[4] More details about P_{rad} and P_{solar} will be discussed in section Radiative Cooling Materials, and $P_{non\text{-}rad}$ will be discussed in section Mid-IR Transparent Thermal Insulator.

There are mainly two kinds of radiative cooling materials according to their spectral properties: selective radiation and broadband radiation[4,30] (Figure 2b). According to Planck's blackbody radiation law (eq 2), to achieve a large radiation power, a surface should have ε close to 1 for all wavelengths except the solar spectrum to avoid the heat gain from the sun (eq 4). However, based on Kirchhoff's radiation law (3), for sub-ambient cooling, broadband high emissivity will result in extra incoming radiative power from the ambient atmosphere, which will limit the temperature drop of the cooling material. Therefore, in order to achieve a significant temperature drop, radiative cooling materials need to be designed to be spectrally selective in the atmospheric window and directly emit the thermal radiation to the cold universe. In other words, selectively emitting surfaces can achieve a more substantial sub-ambient temperature drop, while the broadband surfaces have a larger net cooling power when the temperature of the cooling object is higher or only slightly lower than the ambient. For example, Eriksson et al.[30] reported that the temperature difference between the cooling device and the environment (ΔT) of selective radiation materials is twice as high as the temperature difference of normal blackbody radiation materials. Specifically, if we neglect the non-radiation loss, ΔT can be 14−26 °C for the blackbody surface and 27−62 °C for selective radiation. If $P_{non\text{-}rad}$ is taken into consideration, ΔT is

https://dx.doi.org/10.1021/acsmaterialslett.0c00322
ACS Materials Lett. 2020, 2, 1624−1643

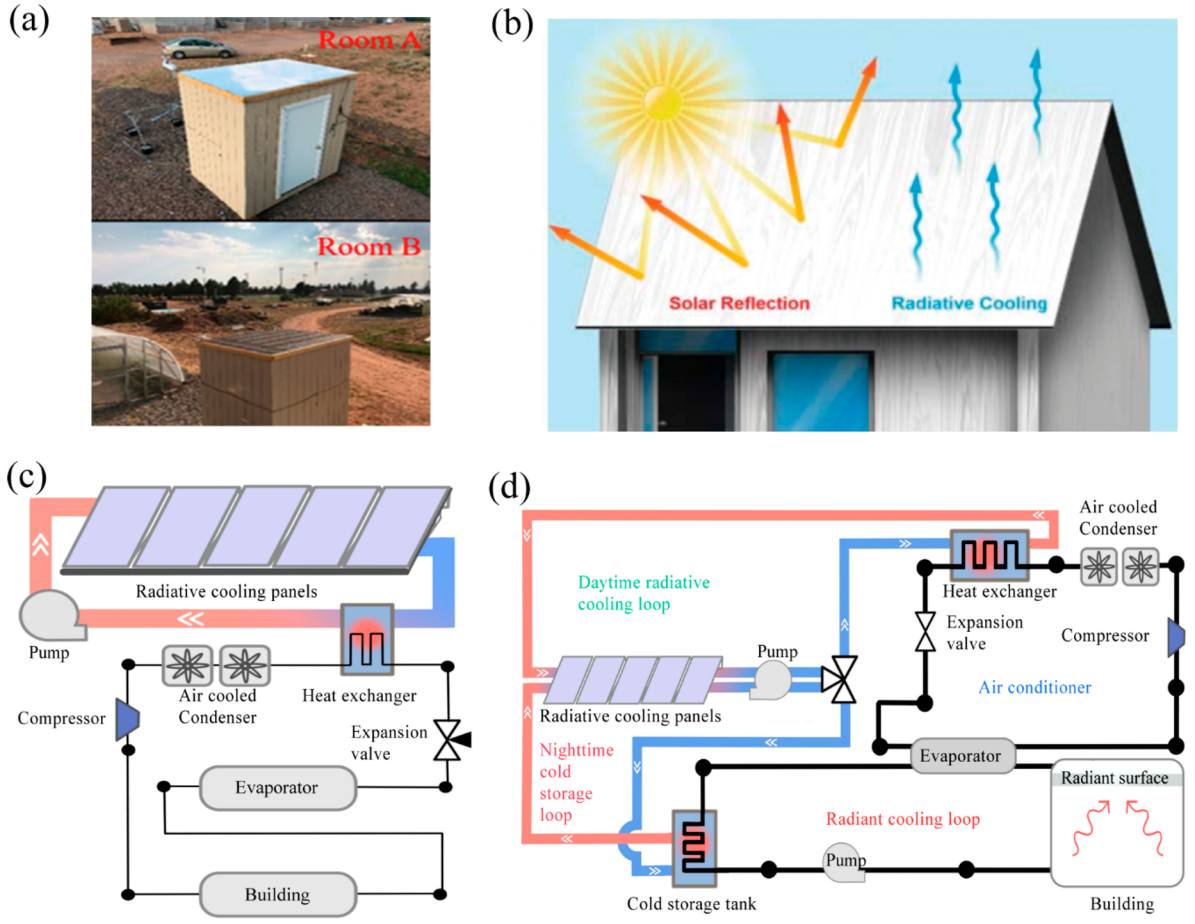

Figure 3. Radiative cooling devices. (a) Comparison study of a radiative cooling roof and a regular shingle roof. Reprinted with permission from ref 13. Copyright 2019 Elsevier. (b) Wood-based building material for radiative cooling. Reprinted with permission from ref 18. Copyright 2019 American Association for the Advancement of Science. (c) A daytime radiative sky cooling system for improving air-conditioner efficiency by cooling condenser. Reprinted with permission from ref 5. Copyright 2017 Nature Publishing Group. (d) A radiative cooling system with a cold storage tank for improving air-conditioner efficiency by cooling condenser.

still 18−33 °C for selective radiation, which is nearly twice as high as ΔT for the blackbody surface (11−21 °C). In practice, both selective and broadband blackbody radiation surfaces have their own suitable applications. In the scenarios where the high cooling power P_{rad} is preferred over sub-ambient cooling such as solar cell cooling, broadband radiative cooling materials have their advantages. On the other hand, selective radiation materials are more suitable when a lower surface temperature is preferred, such as radiant cooling and refrigeration.

■ RADIATIVE COOLING MATERIALS

Based on the above model analysis, high daytime radiative cooling power requires materials with high solar reflectance (usually >95%) and high mid-IR emission (8−13 μm). According to the different strategies for sunlight reflection, daytime radiative cooling materials can be divided into two categories. One is based on silver (Ag)/aluminum (Al) film to achieve high solar reflectance (Figure 2c). In this case, photonic crystals[3,16] or polymers[5,13−15,23,26,27] with transparency in the visible region and high emissivity in the mid-IR region (such as TiO_2/TPX polymer, PTFE, PDMS) were selected and coated on the surface of Ag/Al film to achieve high solar reflectance and mid-IR emission simultaneously (see Table 1). For example, Zhai et al.[23] developed a cooling material that embedded randomly distributed resonant polar dielectric microspheres (micrometer-sized SiO_2 spheres) in a matrix material of polymethylpentene as the mid-IR emitter. The back reflector is 200 nm Ag film. The result shows that about ∼96% solar irradiation and over >93% emissivity between 8 and 13 μm can be achieved. The testing result shows that over 100 W/m^2 radiative cooling power under direct sunlight at room temperature can be obtained. Zhou et al.[27] designed the cooling material that consists of 150 μm thick PDMS film on Al film. The results show over 90% reflection of solar energy and about 94.6% emissivity between 8 and 13 μm, yielding over 120 W/m^2 radiative cooling power. The other one is based on multiscale pores, channels, and/or fibers of cooling materials to efficiently scatter the sunlight (Figure 2d). In this case, the base materials (such as wood[18] and poly(vinylidene fluoride-*co*-hexafluoropropene)[20]) themselves have strong mid-IR emissivity (see Table 1). For example, Mandal et al.[20] presented the hierarchically porous poly(vinylidene fluoride-*co*-hexafluoropropene) (P(VdF-HFP)HP) can achieve 96% solar reflectance and 97% emissivity between 8 and 13 μm. The result shows that about 96 W m^{-2} cooling power can be achieved under solar intensities of 750 W m^{-2}. Li et al.[18] demonstrated a wood-based cooling material by complete delignification of wood. The result shows that the wood-based cooling material is able to achieve 96% solar reflectance and over 90% emissivity

https://dx.doi.org/10.1021/acsmaterialslett.0c00322
ACS Materials Lett. 2020, 2, 1624−1643

between 8 and 13 μm, yielding 63 and 16 W/m^2 cooling powers during the night and daytime (between 11 a.m. and 2 p.m.) and 53 W/m^2 average cooling power over the 24 h period.

It is worth noting that the cooling power is dependent not only on the materials' properties but also on the climate conditions (more details can be seen in the Theoretical Model part). Therefore, the reasonable way to compare the performances of these radiative cooling materials is to take the theoretical values of the corresponding weather conditions into account, rather than comparing only the absolute values of cooling powers. Besides performance, cost analysis and environmental stability are also crucial figures of merits for real applications, which is less discussed at the current stage. We believe it is necessary to consider them in the future design.

MID-IR TRANSPARENT THERMAL INSULATOR

Besides optical properties, the above model also indicates that non-radiative loss needs to be suppressed to achieve significant cooling. Typically, a layer of IR transparent material was selected as a convection shield between radiation materials and ambient. For example, Zhao et al.[26] found the h without a convection shield can be expressed as $h = 8.3 + 2.5V_{wind}$ and h with a convection shield (polyethylene (PE) film, air gap thickness of 1.5 cm) can be expressed as $h = 2.5 + 2.0V_{wind}$, where V_{wind} (m/s) is the zero-incidence wind velocity. It is worth noting that the h should be case-specific due to the different convection shield structures and the air gap thickness between the convection shield and the radiation surface. In addition to PE,[23,26] ZnSe[12] has also been demonstrated as a mid-IR transparent shield. ZnSe has very high transmittance in the 8−13 μm range (about 90% transmittance at 0.32 in. thickness) and is mechanically strong to be used for vacuum chambers in which convection was eliminated, and deep sub-ambient cooling was achieved. However, the cost of ZnSe windows is prohibitively high, which is challenging to be used at the building scale.

To obtain more substantial cooling without using vacuum chambers, simple convection shields are not enough. The inner air convection between cooling materials and IR transparent material will become the dominant heat loss (h only can suppress to 3−10 W/m^{2}K in this situation), which limits the minimum achievable temperature to only about 10 °C below ambient.[17] To further decrease h, the conduction and convection between the radiation material and ambient should also be suppressed without sacrificing the radiative cooling power. As shown in Figure 2e, Leroy et al.[17] developed a PE aerogel, which can achieve 92.2% solar reflectance and 79.9% transmittance between 8 and 13 mm at 6 mm thick and low thermal conductivity (k = 28 mW/mK). By adding 18 mm of PE aerogel on top of the emitter, they can reduce h from 12.9 to 1.4 W/m^{2}K by suppressing the air convection between cooling materials and ambient. The result shows that 13 °C below ambient temperature can be obtained. Moreover, they suggest alternative IR transparent materials, such as BaF_2 and ZnS, could be explored to achieve better optical and thermal performance.

PASSIVE DAYTIME COOLING DEVICE

Besides the development of cooling materials, the design and control of devices and systems according to different weather conditions also play a vital role. This section will focus on the passive device first. Note that the term "passive" means there is zero energy input during device operation. Currently, the passive device can be mainly divided into two categories according to their application types. The first one is to use cooling materials as paint to cover the building envelope for cooling. Fang et al.[13] designed three reduced-size model building (width 2.44 m, length 1.83 m, height 2.44 m, Figure 3a) with daytime radiative cooling material (glass−polymer hybrid metamaterial, about 96% solar irradiation reflection and the emissivity is over >93% between 8 and 13 μm) roof and a commercial roof (the thermoplastic polyolefin roof) and tested the cooling effect in three locations in the United States (Tucson, AZ, Los Angeles, CA, and Orlando, FL). The result shows that the energy savings from utilizing daytime cooling material can reach 113.0−143.9 kWh/(m^2·yr) compared to the thermoplastic polyolefin roof of 88.0−92.4 kWh/(m^2·yr) for the three analyzed locations. The other one is to use cooling materials as the building structural material. Li et al.[18] developed a wood-based daytime radiative cooling material, which not only can achieve high cooling performance (see section Radiative Cooling Materials) but is also 8.7 times as strong and 10.1 times as tough as natural wood. The strong mechanical properties allow the cooling wood to be used as both roof and siding material without other mechanical support (Figure 3b). The results of EnergyPlus simulation show that an average of 35% in cooling energy savings can be obtained for old midrise apartment buildings (before 1980) and an average of about 20% can be obtained for new midrise apartments (after 2004) in the United States. Moreover, the results show that the highest energy saving is appearing in southwest cities, such as Austin, Honolulu, Las Vegas, Atlanta, and Phoenix, because of its hot and dry climate. Passive systems are simple to apply without extra energy input. However, it only improves building energy efficiency in hot weather and can cause excessive cooling during cold weather when the cooling demand is low or even undesirable.

ADAPTIVE DAYTIME COOLING DEVICE

Compared with passive devices, active systems are more complicated but have versatile controllability of transport of cooling power. Based on different heat transfer media, the current adaptive devices can be divided into air-based and water-based daytime radiative cooling systems. For air-based daytime radiative cooling systems, with sub-ambient radiative cooling of air during the day, the temperature of the ventilation air into the indoor can be reduced. Zhao et al.[25] demonstrated a daytime radiation air cooler with a size of 1.84 m by 0.58 m based on glass−polymer hybrid metamaterial (about 96% solar irradiation reflection and the emissivity is over >93% between 8 and 13 μm). The result shows that the radiative air cooler can cool the intake outdoor air by 2−3 °C lower than the ambient temperature at noon under a flow rate of 7.9 L/(m^2 s) in a typical summer day with clear sky conditions.

Water-based daytime radiative cooling systems usually can obtain more energy savings.[4] As shown in Figure 3c, Goldstein et al.[5] used daytime radiative cooling to cool the condenser of the air conditioners to improve the air conditioner's efficiency. In general, the electricity consumption of the air conditioner can be reduced by 3−5% when the condenser temperature decreases 1 °C. They constructed circulated daytime radiative water cooling panels and achieved a temperature reduction of 3−5 °C under a water flow rate of 0.2 L/(min m^2). The

https://dx.doi.org/10.1021/acsmaterialslett.0c00322
ACS Materials Lett. 2020, 2, 1624−1643

Table 2. Summarization of the Smart Window Works

class	materials	performance	cycling	tuning range	reference
electrochromics	porous WO_3 film	ΔT_{633nm}, 97.7%	300	visible and visible/near-IR simultaneous tuning	33
electrochromics	WO_3 nanowire array	ΔT_{750nm}, 43% ΔT_{2000nm}, 62%	2500	visible and visible/near-IR simultaneous tuning	40
electrochromics	Bi and Cu (electrodeposition)	ΔT_{vis}, ~65%	4000	visible and visible/near-IR simultaneous tuning	47
electrochromics	dye-doped (nondichroic dye (LT1641B) and dichroic dye (RL002)) polymer-stabilized liquid crystals	ΔT_{vis}, 85%	none given	visible and visible/near-IR simultaneous tuning	50
electrochromics	SnO_2–WO_3 core–shell structure	ΔT_{1200nm}, 62%	300	near-IR tuning	42
electrochromics	polythiophenes and tin-doped indium oxide	ΔT_{700nm}, 47% ΔT_{1250nm}, 39%	200	visible/near-IR independent tuning	44
electrochromics	Ta-doped TiO_2 nanocrystals	bright mode, T_{vis}, 93.4% T_{NIR}, 94.4% cool mode, T_{vis}, 70.1% T_{NIR}, 18.3% dark mode, T_{vis}, 4.3% T_{NIR}, 17.5%	30	visible/near-IR independent tuning	45
thermochromics	ionic liquid–nickel–chlorine combined with VO_2	ΔT_{solar}, 26.45%	none given	visible tuning	54
thermochromics	mix of methylammonium (MA) iodide, MABr, $PbBr_2$, PbI_2 solution	yellow, orange, red, black color	7	visible tuning	56
thermochromics	SiO_2/VO_2 core/shell 2D photonic crystal	ΔT_{2500nm}, 70%	60	near-IR tuning	57
thermochromics	VO_2/TiN	ΔT_{2000nm}, ~48%	none given	near-IR tuning	59
thermochromics	Cs_xWO_3 nanorods with a layer of poly(vinylpyrrolidone)	ΔT_{vis}, 65.5% ΔT_{IR}, ~20%	200	visible/near-IR simultaneous tuning	61
thermochromics	pNIPAm-AEMA	ΔT_{solar}, 81.3% ΔT_{IR}, 75.6%	1000	visible/near-IR simultaneous tuning	62
mechanochromics	wrinkles on top of PDMS film, silica particles embedded inside	ΔT_{550nm}, ~70.8% with additional 30% strain	none given	visible tuning	64
mechanochromics	poly(dimethylsiloxane)	26% electricity savings when used as a building envelope	none given	visible tuning	67
mechanochromics	porous polymer coatings with fluids like alcohol or water	ΔT_{solar}, ~33% $\Delta T_{8-13\mu m}$, ~64%	100	visible/mid-IR independent tuning	70
thermomechanical system	elastomeric metamaterial containing phase change VO_2 nanoparticles	ΔT_{solar}, 37.7% ΔT_{1260nm}, 33.2%	100	visible/near-IR simultaneous tuning	69
photochromics	tungsten oxide/3-(triethoxysilyl)propyl methacrylate/tetraethoxysilane hybrid xerogels	colorless → blue	10	visible tuning	71

EnergyPlus model shows about 21% reduction in electricity consumption for space cooling. A hybrid radiative cooling system combines the cooling system and the cold storage tank to regulate the difference between supply and demand of daytime and nighttime for higher efficiency. As shown in Figure 3d, Zhao et al.[26] demonstrated daytime radiative cooling water cooling panels combined with a storage system. In this system, daytime and nighttime radiative cooling are separate. During the daytime, the cooling water is used to directly cool the condenser, while, at night, the cooling energy stores into the storage unit, which is retrieved during the daytime to reduce the cooling load on air conditioners. The result shows that a temperature reduction of about 3.1 °C under a water volumetric flow rate of 26.5 L/(h m^2) can be obtained. In addition, the EnergyPlus and Matlab model result shows that, for three different locations (Phoenix, Houston, and Miami) in the United States, the system could potentially save 64–82% of the electricity consumption for cooling in winter (from November to February) and save 32–45% of the electricity consumption for cooling in summer (from May to August). Even though the adaptive device has achieved significant progress, in order to attain all-year-round energy saving under spatial and temporal variation of the weather conditions, dynamic tuning of heating and cooling of roof technology is highly desirable.

SMART WINDOW

Smart windows refer to the window that light transmission properties can be dynamically modulated by stimuli such as voltage, heat, and light. The corresponding technologies are named electrochromic, thermochromic, and photochromic windows, respectively.[6,31,32] In general, the glass changes from transparent to translucent or opaque, thereby changing electromagnetic energy flowing into the building (see Table 2).

https://dx.doi.org/10.1021/acsmaterialslett.0c00322
ACS Materials Lett. 2020, 2, 1624–1643

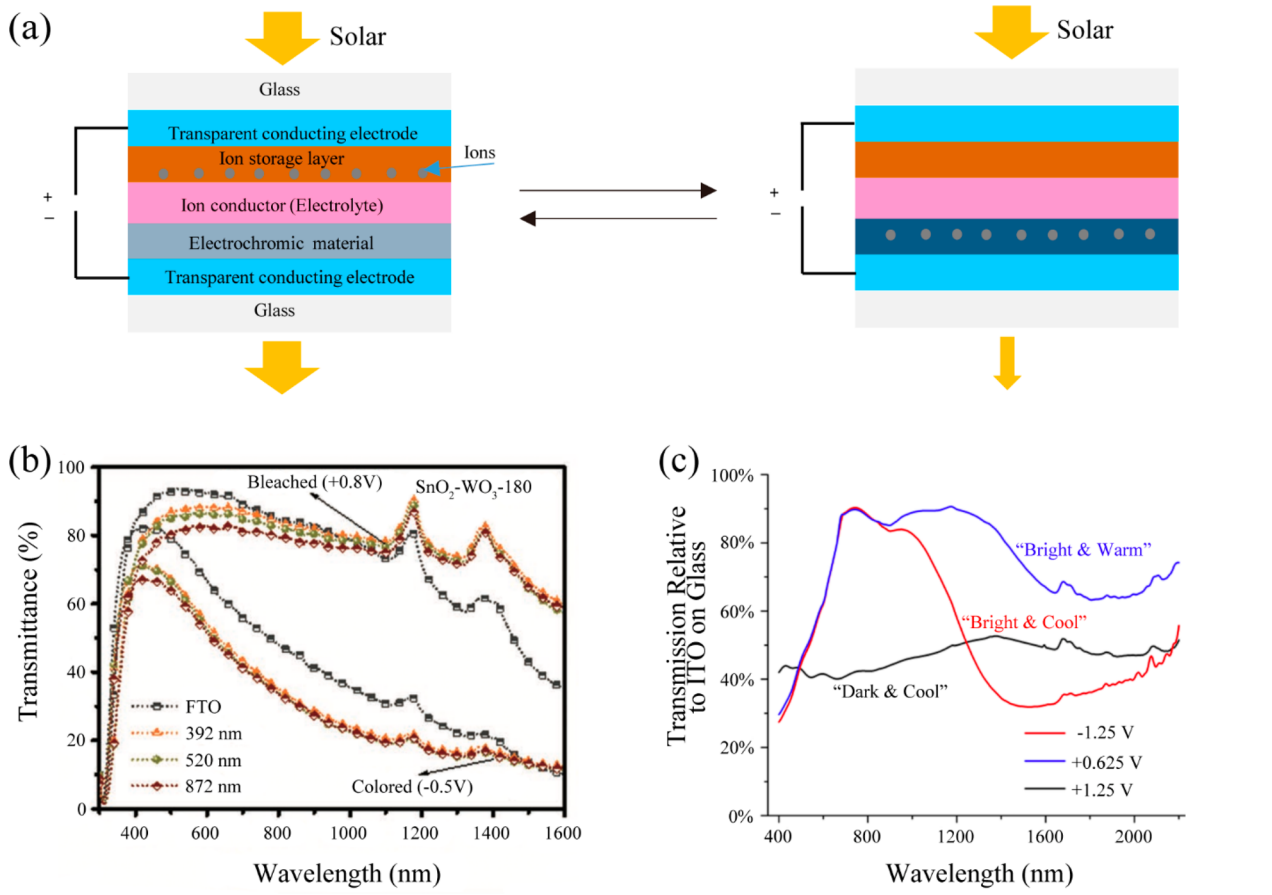

Figure 4. (a) Schematic of the electrochromic window based on electrochromic materials. (b) Transmittance spectrum of the SnO_2−WO_3 core−shell IO structure in the bleached and colored state at different thicknesses of the SnO_2 layer. Reprinted with permission from ref 42. Copyright 2019 Wiley-VCH Verlag GmbH & Co. (c) Transmission spectra of the Pme_2T_2−ITO composite material polarized at −1.25 V (red), +0.625 V (blue), and +1.25 V (black) over wavelength. Reprinted with permission from ref 44. Copyright 2016 American Chemical Society.

■ ELECTROCHROMISM

Electrochromic windows provide reversible and fast optical switching between the clear and dark states upon application of voltage. Compared to other smart window technologies, one significant advantage is that electrochromic windows have uniform optical properties in different states.[32] Electrochromic materials,[33−43] such as inorganic metal oxides (WO_3, NiO, MoO_3) and organic polymers (polyaniline (PANI), polypyrrole (PPy)), reversible electrodeposits,[44−48] and liquid crystal,[49−52] are the most commonly studied types of materials. Aside from visible light tuning, the above-mentioned strategies also can achieve visible and near-IR tuning simultaneously, and some can independently modulate the visible and near-IR (see below).

Visible and Visible/Near-IR Simultaneous Tuning. (1) Based on electrochromic materials: An electrochromic window contains two transparent conducting electrodes separated by the electrolyte. One or both of the transparent conducting electrodes contain an electrochromic material, which changes its color upon application of a voltage (Figure 4a). Specifically, the transmission change is caused by the redox reaction of the electrochromic material upon electrically induced cation (such as H^+, Li^+) insertion/extraction. Cai et al.[33] reported a porous and interconnecting WO_3 network prepared by the pulsed electrochemical deposited method that achieves 97.3% optical modulation at 633 nm, fast switching speed (6 s of coloration and 1.9 s of bleaching), and excellent cycling stability (almost unchanged over 300 cycles). The result shows that the performance is much better than the compact film. The reason is very similar to battery electrode engineering, in which porous structures not only facilitate electrolyte penetration and ion transport but also alleviate WO_3 expansion. Xia et al.[40] designed an electrochromic device that is composed of a reduced graphene oxide-connected bilayer NiO nanoflake array cathode and a WO_3 nanowire array anode. The result shows that it not only induced a change in visible light from transparent to blue but also up to 62% near-IR modulation from 1000 to 2000 nm. (2) Based on electrodeposition: Electrodeposition based smart window is the reversible electrochemical deposition and etching of metals, such as Ag, Cu, and Bi, between the two electrodes. The device also consists of two transparent conducting electrodes located on opposite sides of the transparent electrolyte. The metal cations coming from electrolyte will be reduced to form a solid film on the transparent conducting cathode to achieve the opaque state, and the reverse oxidation process can recover back to the transparent state. Islam et al.[47] designed a smart window that combines reversible Bi and Cu electrodeposition with lithium-ion insertion in a NiO counter electrode. About 65% of optical modulation at 600 nm in 1 min can be achieved. Moreover, the result shows that over 4000 times cycle can be achieved after introducing a N5-benzyl-1*H*-1,2,4-triazole-3,5-diamine to

https://dx.doi.org/10.1021/acsmaterialslett.0c00322
ACS Materials Lett. 2020, 2, 1624−1643

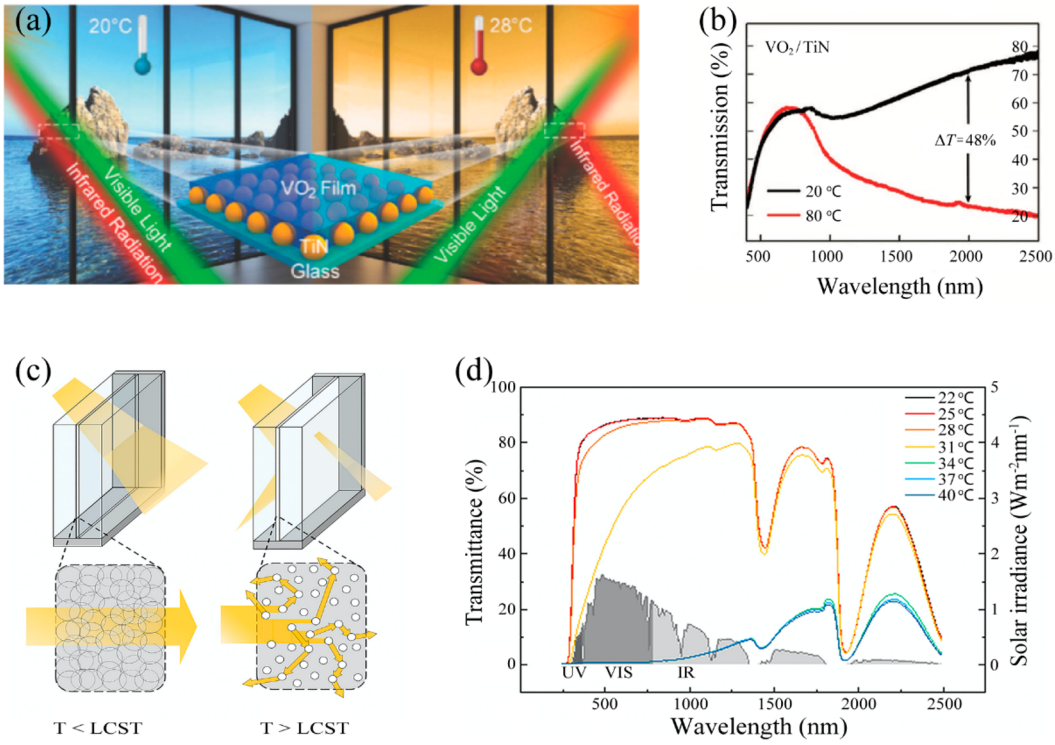

Figure 5. (a) Schematic representation of hybrid VO_2/TiN material applied as a smart window. Reprinted with permission from ref 59. Copyright 2018 Wiley-VCH Verlag GmbH & Co. (b) Transmission spectra of the VO_2/TiN materials at temperatures of 20 and 80 °C. Reprinted with permission from ref 59. Copyright 2018 Wiley-VCH Verlag GmbH & Co. (c) Schematic of the regulatory mechanism of pNIPAm-AEMA. Reprinted with permission from ref 62. Copyright 2019 Elsevier. (d) Transmittance spectra of pNIPAm−AEMA hydrogel with a layer thickness of 240 μm over wavelength at different temperatures. The inset is the solar irradiance spectrum (gray area). Reprinted with permission from ref 62. Copyright 2019 Elsevier.

prevent metal growth on the NiO counter electrode. (3) Based on liquid crystal: Liquid-crystal-based devices change their transmittance by rotating the liquid crystals to scatter/absorb the light. Sun et al.[50] reported dye-doped (nondichroic dye (LT1641B) and dichroic dye (RL002)) polymer-stabilized liquid crystals, which can tune from 95 to 10% (during 400−800 nm) specular transmittance upon application of 30 V voltage.

Near-IR Tuning. Near-IR light accounts for 43% of sunlight energy. Sometimes, in order to achieve the bright while suppressing the heat effect according to personal preference and energy-saving needs, selective modulation of the near-IR is critical.[42] Nguyen et al.[42] selected highly transparent SnO_2 inverse opal (IO) as the framework to electrochemically deposit an amorphous WO_3 layer to form a hybrid SnO_2−WO_3 core−shell IO structure. As shown in Figure 4b, the result shows that a SnO_2 (392 nm)−WO_3 (180 nm) core−shell structure can achieve effective near-IR modulation (62% at 1200 nm) while maintaining about 70% visible light transparency and about 15% drop in near-IR blocking after 300 cycles. The result also shows that the core−shell IO structure not only promotes the electrochromic kinetics of WO_3 but also enhances the photonic crystal effect on the near-IR range absorption. Both of them are beneficial for tuning of near-IR.

Visible/Near-IR Independent Tuning. Aside from mainly tuning the near-IR, impressive works were also reported to accomplish selective and independent tuning of visible and near-IR.[43] For example, Barile et al.[44] reported a class of hybrid electrochromic materials using polythiophenes and tin-doped indium oxide (ITO) nanoparticles that can selectively modulate the visible light and near-IR to achieve three modes: "bright and warm", "bright and cool", and "dark and cool" (Figure 4c). At −1.25 V, the poly(3,3′-dimethyl-2,2′-bithiophenyl) (Pme_2T_2)−ITO electrodes are in a "bright and cool" state because the Pme_2T_2 is light yellow, and the ITO nanoparticles absorb near-IR light. Upon increasing the polarization of the electrode to +0.625 V, the electrode switches to a "bright and warm" state because the Pme_2T_2 remains light yellow, but the ITO nanoparticles do not absorb near-IR light as strongly. When the voltage is increased to +1.25 V, the film enters a "dark and cool" state because the Pme_2T_2 film becomes dark blue and relatively opaque to 700 nm light and polarons in Pme_2T_2 absorb the near-IR. The result shows that the maximum contrast ratios of the composite systems are 47% at 700 nm and 39% at 1250 nm, and about 15−20% contrast ratios degrade after 200 switching cycles. Cao et al.[45] designed a Ta-doped nano-TiO_2 electrode, which can also achieve these three modes. In the "bright and warm" mode at 3.5 V, the electrode was transparent to both visible (93.4%) and near-IR (94.4%) light. In the "bright and cool" mode at 1.8 V, the electrode blocked 81.7% of the near-IR while maintaining 70.1% of visible transmittance. The near-IR transmittance decrease in this mode could be attributed to the increase of free charge carriers in Ta-doped TiO_2, which generated a localized surface plasmon resonance absorption in the near-IR region through capacitive charging. The "dark and cool" mode was activated by Li^+ intercalation into the TiO_2 host at 1.5 V. The electrode film was completely dark and blocked 95.7% of visible light and 82.5% of near-IR.

https://dx.doi.org/10.1021/acsmaterialslett.0c00322
ACS Materials Lett. 2020, 2, 1624−1643

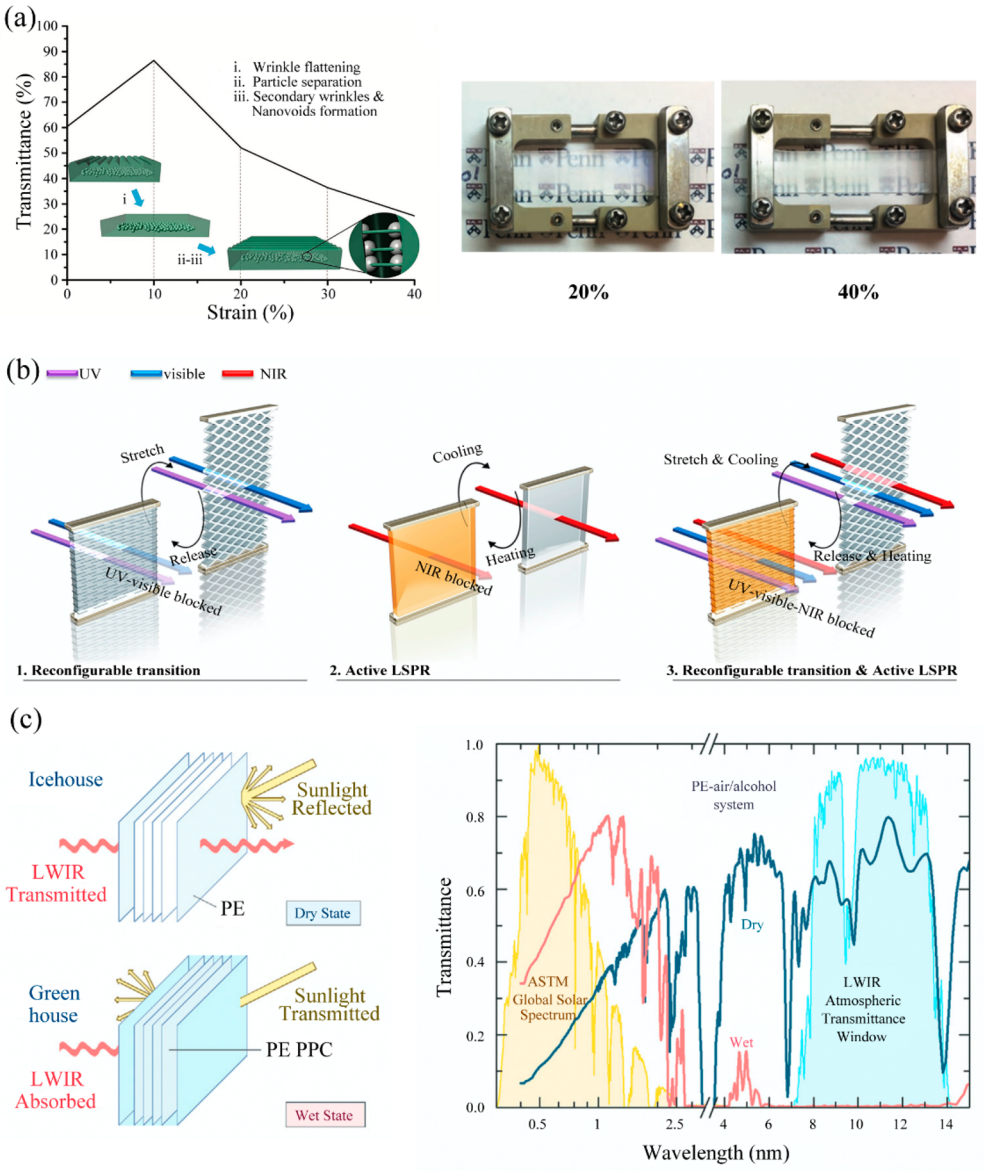

Figure 6. (a) Transmittance spectrum (550 nm) of wrinkle silica NP composite film (pre-strain: 10%) over the strain (0−40%). Reprinted with permission from ref 64. Copyright 2018 Wiley-VCH Verlag GmbH & Co. (b) Schematic of the transmittance of the regulatory mechanism based on reconfigurable metamaterials, active LSPR, and the integration of active LSPR and reconfigurable metamaterials. Reprinted with permission from ref 69. Copyright 2019 Elsevier. (c) Icehouse-to-greenhouse switching of a PE-air/alcohol system (left); transmittance spectrum of the wet and dry states of the PE-air/alcohol system (right). Reprinted with permission from ref 70. Copyright 2019 Elsevier.

■ THERMOCHROMISM

Thermochromic windows change the transmittance according to the ambient temperature. They have high transparency in cold weather to allow the solar radiation to enter the building for heating and low transparency in hot weather to block the solar light for cooling.[6,53] Compared with electrochromic windows, one of its distinctive features is that it does not require electricity or additional control systems, which makes it much easier to install. However, compared with electrochromism, thermochromism sacrifices the capability of on-demand control. The weather conditions control it, and the residents cannot make any adjustments to suit their preferences. Examples are ionic liquids,[54,55] perovskites,[56] vanadium dioxide,[57−60] liquid crystals,[61] and hydrogels.[62] Among them, ionic liquids and perovskites so far can only tune the visible light, vanadium dioxide is suitable for tuning near-IR, and hydrogels and liquid crystals can achieve the simultaneous tuning of visible and near-IR. Their switching mechanisms are explained below.

Visible Tuning. (1) Ionic liquid. Zhu et al.[54] reported the material composed of di-(1-butyl-3-methyl-imidazolium) ($[bmim]_2NiCl_4$) dissolved in an ionic liquid, 1-(3-hydroxyethyl)-3-methylimidazolium tetrafluoroboride ($C_2OhmimBF_4$). When the temperature increases from 20 to 80 °C, the ionic liquid−nickel−chlorine (IL−Ni−Cl) complexes absorb increasing visible light (≈680 nm) and gradually change color from colorless to blue. In the system, the octahedral $[NiCl_{6-x}(C_2OhmomBF_4)]_{x-4}$ shows a reversible ligand exchange process to the $C_2Ohmim\ BF_4$ under elevated

https://dx.doi.org/10.1021/acsmaterialslett.0c00322
ACS Materials Lett. 2020, 2, 1624−1643

temperature, with the corresponding reaction formula as shown below:

$$[NiCl_{6-x}(C_2OHmimBF_4)_x]^{x-4} + (x-2)Cl^- \rightleftharpoons [NiCl_4]^{2-} + xC_2Ohmim \quad (\text{where } 0 < x \leq 2) \tag{6}$$

(2) Perovskite materials. De Bastiani et al.[56] reported a perovskite ink, which can achieve reversible thermochromic changing from yellow to black as the temperature increases from 25 to 120 °C. At room temperature, the mix of methylammonium (MA) iodide, MABr, $PbBr_2$, and PbI_2 solution is pale yellow color. When the temperature is increased to 60 °C, $MAPbBr_{2.7}I_{0.3}$ is formed and turns orange color. By further increase of temperature, the rapid drop of $MAPbI_3$ solubility results in more incorporation of iodine, generating red $MAPbBr_{2.4}I_{0.6}$ at 90 °C and black $MAPbBr_{1.8}I_{1.2}$ at 120 °C.

Near-IR Tuning. Vanadium dioxide (VO_2) is a typical thermochromic material that changes its near-IR transparency at phase change temperature (68 °C) as well as maintaining transmittance in the visible range.[57−60] Ke et al.[57] reported a SiO_2/VO_2 core/shell 2D photonic crystal, which can achieve about 70% contrast at 2500 nm with 49% visible transmittance when the temperature switches between 20 and 90 °C. However, the phase transition temperature of VO_2 is too high for building heat management (20−40 °C), so strategies such as doping and hybridization are often used to reduce its phase transition temperature.[58] For example, Hao et al.[59] designed a hybridizing thermochromic VO_2 with plasmonic TiN nanoparticles (Figure 5a). In this system, the TiN particles can convert near-IR light to heat and accelerate the phase transition of VO_2. Thus, it can achieve phase change and blocks about 70% IR light under strong illumination (300 mW cm^{-2}) at 28 °C. Instead, it is near-IR transparent under weak irradiation density or at a low temperature of 20 °C. The result shows that the near-IR light modulation can reach to 48% at 2000 nm with 51% visible transmittance (Figure 5b).

Visible/Near-IR Simultaneous Tuning. (1) Liquid crystal. Thermal-responsive liquid crystals were developed to simultaneously tune the visible and near-IR for the smart window. One typical type is based on the reversibly crystal orientation transition between the smectic (SmA) and chiral nematic (N*) phases. Liang et al.[61] reported a polymeric syrup containing liquid crystals with a smectic A (SmA) to chiral nematic (N*) phase transition that is able to achieve about 65.5% visible tuning and about 20% near-IR tuning. (2) Hydrogel. Hydrogels with the lower critical solution temperature (LCST) behavior are transparent at low temperatures but become strongly scattering at high temperatures because of the aggregating of polymer microparticles. Most recently, as shown in Figure 5c and d, Li et al.[62] demonstrated a new type of thermochromic, poly(*N*-isopropylacrylamide)-2-aminoethyl-methacrylate hydrochloride (pNIPAm-AEMA) microparticles, which are able to tune the light-scattering behaviors by controlling the particle size and internal structure. The average size of pNIPAm-AEMA microparticles changes from 1388 to 546 nm when the temperature increases from 25 at 35 °C, yielding 81.3% visible modulation and 75.6% near-IR transmittance modulation.

MECHANOCHROMISM AND PHOTOCHROMISM

Mechanochromism[63−70] and photochromism[71−74] are the other two important categories, although in a relatively early stage of development. Just as other active tuning approaches, mechanochromism generally has a larger tuning range. Specifically, by integrating with other strategies (e.g., thermochromics) or IR transparent materials, the multispectral tuning of mechanochromism can expand from visible to near-IR or mid-IR.

Visible Tuning. The mechanochromic smart window is also a common strategy for tuning visible light by mechanical strain with the advantages of simple construction, low cost, and fast response time. There are several ways to actuate the strain, and this review will focus on the surface wrinkling and Kirigami structures for their superior performances. (1) Surface wrinkling. Cyclic mechanical strain is applied to reversibly induce and remove the surface wrinkles, which dynamically and continuously tune the light scattering. Kim et al.[64] reported a multistate and on-demand mechanoresponsive smart window, which contains wrinkles on top of the elastomeric poly(dimethylsiloxane) film and a thin layer of silica particles embedded in a poly(dimethylsiloxane) film at the bottom. After optimizing the wrinkle formation, the result shows that about 40 and 70% transmittance change at 550 nm at 20 and 40% strain was achieved (Figure 6a). This larger change is contributed by using the synergetic optical effects from the tunable geometry of wrinkles of the top surface and nanovoids generated surrounding the silica particles embedded in a poly(dimethylsiloxane) film of the bottom surface. (2) Kirigami structures. In general, patterned line cuts or slits are fabricated on a film. The film will break from the originally continuous state (usually opaque state) to discretely connected units (usually transmittance state) when the strain is applied.[67,68] Tang et al.[67] designed a programmable kiri-kirigami structure and investigated its potential application as a smart window for energy saving of building through simulation. The result shows that about 26% of electricity can be saved over the entire year when using the designed kiri-kirigami window.

Photochromism (PC) refers to reversible color change under certain wavelengths of light excitation. It can be categorized into two kinds: organic (naphthopyran, syriopyran, spirooxazine, etc.) and inorganic (WO_3, TiO_2, MoO_3, V_2O_5, metal halides, etc.) PC materials.[6,71−74] Generally, PC materials are embedded or coated onto transparent host materials to be used as a smart window. Among these PC materials, transition metal oxides stand out for superior stability and low cost. WO_3-based materials are the representative category that is most intensively studied. The photochromic chemical reactions of WO_3 are below:

$$WO_3 + h\nu \rightarrow WO_3^* + e^- + h^+ \tag{7}$$

$$h^+ + \frac{1}{2}H_2O \rightarrow H^+ + \frac{1}{4}O_2 \tag{8}$$

$$WO_3 + xe^- + xH^+ \rightarrow H_xWO_3 \tag{9}$$

In the first step, the pairs of the electron (e^-) and hole (h^+) are generated in WO_3 (bleach state) under irradiation ($h\nu$ > the bandgap energy (E_g)). In the second step, the generated h^+ will react with the water, which is absorbed by the WO_3 surface, to form H^+. In the third step, the H_xWO_3 (color state) compound will form by the reaction of WO_3, e^-, and h^+.

https://dx.doi.org/10.1021/acsmaterialslett.0c00322
ACS Materials Lett. 2020, 2, 1624−1643

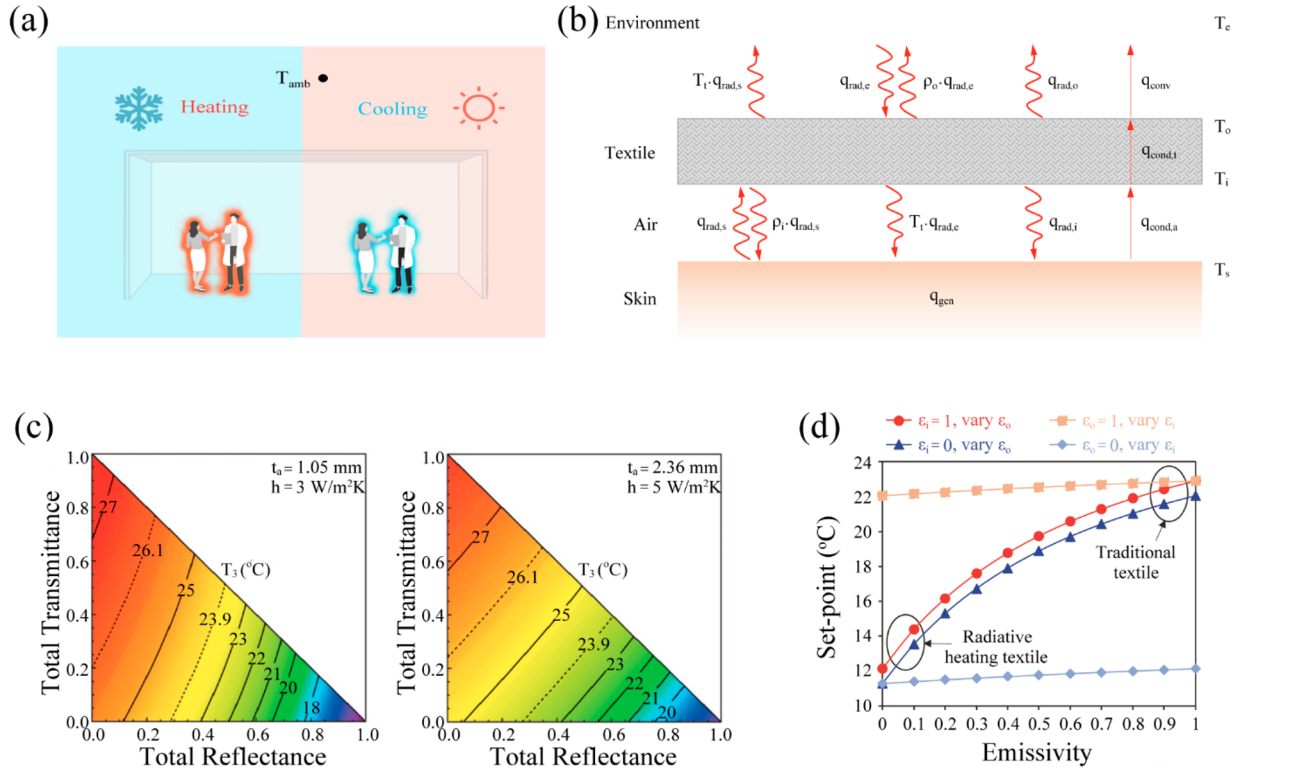

Figure 7. (a) Local thermal environment created around a human body. (b) Schematic of the heat transfer model of the clothed human body. Reprinted with permission from ref 86. Copyright 2017 Nature Publishing Group. (c) The maximum ambient temperature attainable without compromising thermal comfort over the total reflectance and transmittance. Reprinted with permission from ref 85. Copyright 2015 American Chemical Society. (d) The setpoints of ambient temperature for maintaining thermal comfort over the textile's IR emissivity (inner surface (ε_i) and outer surface (ε_o)). Reprinted with permission from ref 86. Copyright 2017 Nature Publishing Group.

However, the performance of pristine WO_3 is not ideal due to its poor revisability and narrow photochromism response range. Doping, structure design, and hybrid methods were designed and implemented to improve its performance. Adachi et al.[71] demonstrated alkali metal cation-controlled silicon oxycarbide/silica hybrid xerogels with a well-dispersed WO_3 nanoparticle hybrid system, which can be triggered by UV light from colorless to blue. Specifically, the pairs of the electron (e^-) and hole (h^+) are generated in WO_3 under irradiation. With the assistance of M^+ (Li^+, Na^+, K^+, Rb^+, and Cs^+ were selected as the charge-compensating cations to insert into the WO_3 frameworks), blue-colored $M_xW_{1-x}{}^{6+}W_x{}^{5+}O_3$ will be generated by reacting of W^{6+} ions (transparent), M^+, and e^- under UV irradiation.

Visible/Near-IR Simultaneous Tuning. Besides visible tuning, mechanochromics also can tune near-IR light by integrating with other strategies,[69,75] such as thermomechanical systems. As shown in Figure 6b, Ke et al.[69] developed a kirigami-inspired elastomeric metamaterial containing phase change VO_2 nanoparticles (NPs) for tuning visible and near-IR to smart windows. On one hand, the UV−visible transmittance can be tuned by stretching and releasing. On the other hand, the near-IR is tuned by localized surface plasmon resonance (LSPR) through the phase change of VO_2, while offering a negligible effect in UV−visible regions. Therefore, by the integration of the active LSPR of VO_2 NPs with the reconfigurable structures, the synergetic thermomechanical system can achieve dynamic tuning of the light transmittance in the UV−visible and near-IR range. The result shows that about 37.7% of solar change can be made by the combined effect of the LSPR and kirigami structures. Meanwhile, the near-IR controllability is enhanced by the assistance of active LSPR; e.g., the contrast at 1260 nm increases from 16.1% on the kirigami sample to 49.3% on the plasmonic kirigami sample.

Visible/Mid-IR Independent Tuning. From the perspective of the energy saving of a building, the regulation of mid-IR can also effectively control the heat radiation of the window. However, glass has strong absorption in the mid-IR, which makes mid-IR regulation of the window difficult. Recently, Mandal et al.[70] demonstrated the visible and mid-IR optical dynamicity that can be achieved by reversibly wetting porous polymer coatings with fluids like alcohol or water (Figure 6c). Specifically, the porous PE shows high reflectance in visible and high transmittance (about 64%) in the mid-IR wavelength because of the appropriate pore size (~0.1 μm) that is too small to scatter thermal IR wavelengths but large enough for visible light scattering. When the isopropanol wets the nanoporous PE and replaces the air void, the refractive index contrast decreases from 0.51 ($n_{PE} - n_{air} = 1.51 - 1.00$) to 0.13 ($n_{PE} - n_{air} = 1.51 - 1.38$) and produces a diffuse transmittance and translucent appearance and an increase of transmittance of 0.33 in the solar spectrum. In the mid-IR region, isopropanol significantly increases the IR absorptivity/emissivity of 0.64. This is the first and very recent work about the opportunity of mid-IR tuning in the smart window, and we believe more works to enhance the performance and stability as well as to understand the relationship between tuning mid-IR and building energy saving are worth further exploration.

https://dx.doi.org/10.1021/acsmaterialslett.0c00322
ACS Materials Lett. 2020, 2, 1624−1643

PERSONAL THERMAL MANAGEMENT

Personal thermal management means heating/cooling the local environment around the human body instead of total building space (Figure 7a), which has the potential to significantly reduce the energy consumption of building for heating and cooling.[7,76−100] In addition, compared to heating/cooling of the entire room, personal thermal management can result in a higher level of thermal comfort satisfaction because of the capability of personalization that tailors to fit the individual preferences.

The cloth between the human body and building is an ideal medium to be designed for personal heat management. There are mainly three attractive personal thermal management technologies based on textile design without power supply.[7,76] The first one is based on the thermal conduction mechanism that tunes the thermal conduction between the human body and the environment by designing high or low thermal-conductivity materials to achieve cooling or heating. The second strategy is based on thermal convection by shape-shifting materials. Last but not least, the third strategy is based on the regulation of electromagnetic radiation, particularly mid-IR thermal radiation. Here, we mainly focus on discussing the strategies based on a mid-IR design clothing system to achieve personal thermal management. Interested readers are referred to recent reviews for exhaustive summaries on the state-of-the-art of personal thermal management based on conduction and convection.[7,76]

It is reported that over 50% of the heat is transported from the textile outer surface to the environment via radiation.[86] There is much space for tuning through material design. Here, a cooling model and a heating model will be discussed to give a systematic understanding of the basic principle of heating and cooling achievement through mid-IR design and provide a guideline for further design of high-performance heating and cooling materials.

In the previous research, the one-dimensional steady-state heat transfer model has been developed and used in personal thermal management design[85,86] (Figure 7b). This model assumes constant skin temperature (33 °C) and the human metabolic heat generation rate (73 W m^{-2}). The criterion for human thermal comfort is the thermal equilibrium between skin and ambient under such conditions. This means the heat generation has to be equal to the heat loss no matter if for heating or cooling purposes. Specifically, in their model, radiation, conduction, and convection are considered to describe the heat dissipation. Based on thermal equilibrium and energy conservation law, the model is described below (the index before the comma represents the input or output heat flux).

On the skin and environment surface (s and e), heat flux could be described as

$$q_{\mathrm{in,s}} + q_{\mathrm{gen}} = q_{\mathrm{out,s}} + q_{\mathrm{cond,a}} \tag{10}$$

$$q_{\mathrm{out,s}} = q_{\mathrm{rad,s}} + (1 - \varepsilon_{\mathrm{s}})q_{\mathrm{in,s}} \tag{11}$$

$$q_{\mathrm{in,e}} + q_{\mathrm{conv}} = q_{\mathrm{out,e}} + q_{\mathrm{gen}} \tag{12}$$

$$q_{\mathrm{out,e}} = q_{\mathrm{rad,e}} + (1 - \varepsilon_{\mathrm{e}})q_{\mathrm{in,e}} \tag{13}$$

where $q_{\mathrm{in,s}}$ and $q_{\mathrm{out,s}}$ are the inward and outward heat flux of the skin, $q_{\mathrm{in,e}}$ and $q_{\mathrm{out,e}}$ are the inward and outward heat flux of the environment, q_{gen} is the metabolic heat generation rate per unit area, $q_{\mathrm{cond,a}}$ is the conductive heat flux in the air gap between the skin and the textile, q_{conv} is the convective heat flux from the textile to the ambient environment, $q_{\mathrm{rad,s}}$ and $q_{\mathrm{rad,e}}$, are the radiative heat flux from the skin and the ambient environment, and ε_{s} and ε_{e} are the IR emittance of the skin and environment. For the textile with inner surface i and outer surface o,

$$q_{\mathrm{out,i}} = q_{\mathrm{rad,i}} + (1 - \tau_{\mathrm{t}} - \varepsilon_{\mathrm{i}})q_{\mathrm{in,i}} + \tau_{\mathrm{t}}q_{\mathrm{in,o}} \tag{14}$$

$$q_{\mathrm{out,o}} = q_{\mathrm{rad,o}} + (1 - \tau_{\mathrm{t}} - \varepsilon_{\mathrm{o}})q_{\mathrm{in,o}} + \tau_{\mathrm{t}}q_{\mathrm{in,i}} \tag{15}$$

where $q_{\mathrm{in,i}}$ and $q_{\mathrm{out,i}}$ are the inward and outward heat flux of the textile inner surface, $q_{\mathrm{in,o}}$ and $q_{\mathrm{out,o}}$ are the inward and outward heat flux of the textile outer surface, $q_{\mathrm{rad,i}}$ and $q_{\mathrm{rad,o}}$ are the radiative heat flux from the textile inner surface and the textile outer surface, τ_{t} is the IR transmittance of the textile, and ε_{i} and ε_{o} are the IR emittance of the textile inner surface and the textile outer surface. The outward and inward heat flux could be written as

$$q_{\mathrm{in,o}} = q_{\mathrm{out,e}} \quad q_{\mathrm{in,i}} = q_{\mathrm{out,s}} \quad q_{\mathrm{in,s}} = q_{\mathrm{out,i}} \quad q_{\mathrm{in,e}} = q_{\mathrm{out,o}} \tag{16}$$

The energy balance equations of the skin surface and textile outer surface are as follows ($\varepsilon_{\mathrm{e}} = 1$)

$$q_{\mathrm{gen}} = (1 - \rho_{\mathrm{i}})[q_{\mathrm{rad,s}} + (1 - \varepsilon_{\mathrm{s}})q_{\mathrm{in,s}}] - \tau_{\mathrm{t}}q_{\mathrm{rad,e}} - q_{\mathrm{rad,i}} + q_{\mathrm{cond,a}} \tag{17}$$

$$q_{\mathrm{gen}} = \tau_{\mathrm{t}}[q_{\mathrm{rad,s}} + (1 - \varepsilon_{\mathrm{s}})q_{\mathrm{in,s}}] - q_{\mathrm{rad,e}} + \rho_{\mathrm{o}}q_{\mathrm{rad,e}} + q_{\mathrm{rad,o}} + q_{\mathrm{conv}} \tag{18}$$

where ρ_{i} and ρ_{o} are the IR reflectance of the textile inner surface and outer surface. With the above formulas, we can derive the temperature distribution inside the textile based on energy conservation law

$$T_{\mathrm{o}} = \frac{t_{\mathrm{t}}}{2k_{\mathrm{t}}}[q_{\mathrm{rad,i}} + q_{\mathrm{rad,o}} - \alpha_{\mathrm{i}}(q_{\mathrm{rad,s}} + (1 - \varepsilon_{\mathrm{s}})q_{\mathrm{in,s}}) - \alpha_{\mathrm{o}}q_{\mathrm{rad,e}}] - \frac{k_{\mathrm{a}}t_{\mathrm{t}}}{k_{\mathrm{t}}t_{\mathrm{a}}}(T_{\mathrm{s}} - T_{\mathrm{i}}) + T_{\mathrm{i}} \tag{19}$$

Based on Fourier's law, Newton's law, and the Stefan−Boltzmann law, the radiation, conduction, and convection in the above equations could be written in detail as below

$$\begin{aligned} q_{\mathrm{rad,s}} &= \varepsilon_{\mathrm{s}}\sigma T_{\mathrm{s}}^4 \\ q_{\mathrm{rad,e}} &= \varepsilon_{\mathrm{e}}\sigma T_{\mathrm{e}}^4 \\ q_{\mathrm{rad,i}} &= \varepsilon_{\mathrm{i}}\sigma T_{\mathrm{i}}^4 \\ q_{\mathrm{rad,o}} &= \varepsilon_{\mathrm{o}}\sigma T_{\mathrm{o}}^4 \\ q_{\mathrm{cond,a}} &= \frac{k_{\mathrm{a}}}{t_{\mathrm{a}}}(T_{\mathrm{s}} - T_{\mathrm{i}}) \\ q_{\mathrm{conv}} &= h(T_{\mathrm{o}} - T_{\mathrm{e}}) \end{aligned} \tag{20}$$

where t_{t} is the IR transmittance of the textile, α_{i} and α_{o} are the IR absorbance of the textile inner surface and outer surface, k_{t} is the thermal conductivity of the textile, t_{a} is the thickness of the air gap between textile and skin, and h is the convective heat transfer coefficient. T_{s}, T_{e}, T_{i}, and T_{o} are the skin,

https://dx.doi.org/10.1021/acsmaterialslett.0c00322
ACS Materials Lett. 2020, 2, 1624−1643

Table 3. Summarization of the Personal Heat Management Works Based on the Mid-IR Design Clothing System

function	materials	material properties	durability, permeability, etc.	reference
cooling (C)	nanoporous PE	77.8% IR transmittance and over 99% visible opacity	air permeability (40−60 $cm^3/s\ cm^2$ Pa); water vapor transmission rate (∼0.016 g/cm^2 h); wicking distance (8.3 mm), and mechanical strength (a strip of 2 cm wide nanoPE mesh, which can endure 45 N of tensile force	87
C	knitted/woven nanoPE microfiber fabric	over 80% IR transparency and ∼90% visible opacity	water vapor transmission rate (0.023 g/cm^2 h); wicking rate (3 cm/30 s); mechanical strength (1.5 cm wide nanoPE fabric can bear a tensile force of about 15 N); durability (the mid-infrared transmittance of nanoPE fabric is almost unchanged after 5 cycles of washing and drying)	90
C	PE textiles with Prussian blue, iron oxide, and silicon	over 80% IR transparency and over 80% visible opacity	maximum tensile force, ∼1.9−2.8 N; stability (only about 3.6% pigment loss after 120 washing cycles)	91
passive heating (PH)	cotton/Ag/PE	98.5% IR reflectivity	water vapor transmission rate (0.012 g/cm^2 h); wicking rate (∼1.3 cm/s); mechanical strength (maximum endurable tensile force of 50 N); durability (the emissivity change of cotton/Ag/PE textile is lower than 10% after 10 cycles of washing)	86
PH	silver nanowires (AgNWs) - coated textile	40.8% IR reflectivity	coating reduces the breathability only by 2%; durability (the resistance decreases during the first 2 cycles and then stabilizes without further decay)	95
PH	silica nanoparticles (NPs)/cotton/cellulose acetate/silver	∼0% IR transmittance	breathability, only ∼4% reduction compared with the normal cotton cloth	96
C+PH (Janus cloth)	Cu/MnO_2/cellulose@layered double hydroxide fiber	heating mode: 43.6% IR emissivity cooling mode: 89.5% IR emissivity	water vapor permeability, 11 $mg/cm^2 \cdot h$; durability (the electrical resistance shows a slight increase after six cycles of cleaning tests)	97
C+PH (Janus cloth)	nanoPE/carbon/copper/nanoPE	heating mode: 30.3% IR emissivity cooling mode: 89.4% IR emissivity	the air and water vapor permeability of the Janus textile are similar to traditional textiles	98
C+PH (mechanical tuning)	styrene−ethylene−butylene−styrene/copper	heating mode (0% strain): 1% IR transmittance cooling mode (100% strain): 39 ± 3% IR transmittance	stability, no degradation in their functionality after > $\sim 10^3$ actuation cycles	99
C+PH (humidity tuning)	triacetate−cellulose bimorph fibers with a thin layer of carbon nanotubes	over 35% IR transmittance change	none given	100

https://dx.doi.org/10.1021/acsmaterialslett.0c00322
ACS Materials Lett. 2020, 2, 1624−1643

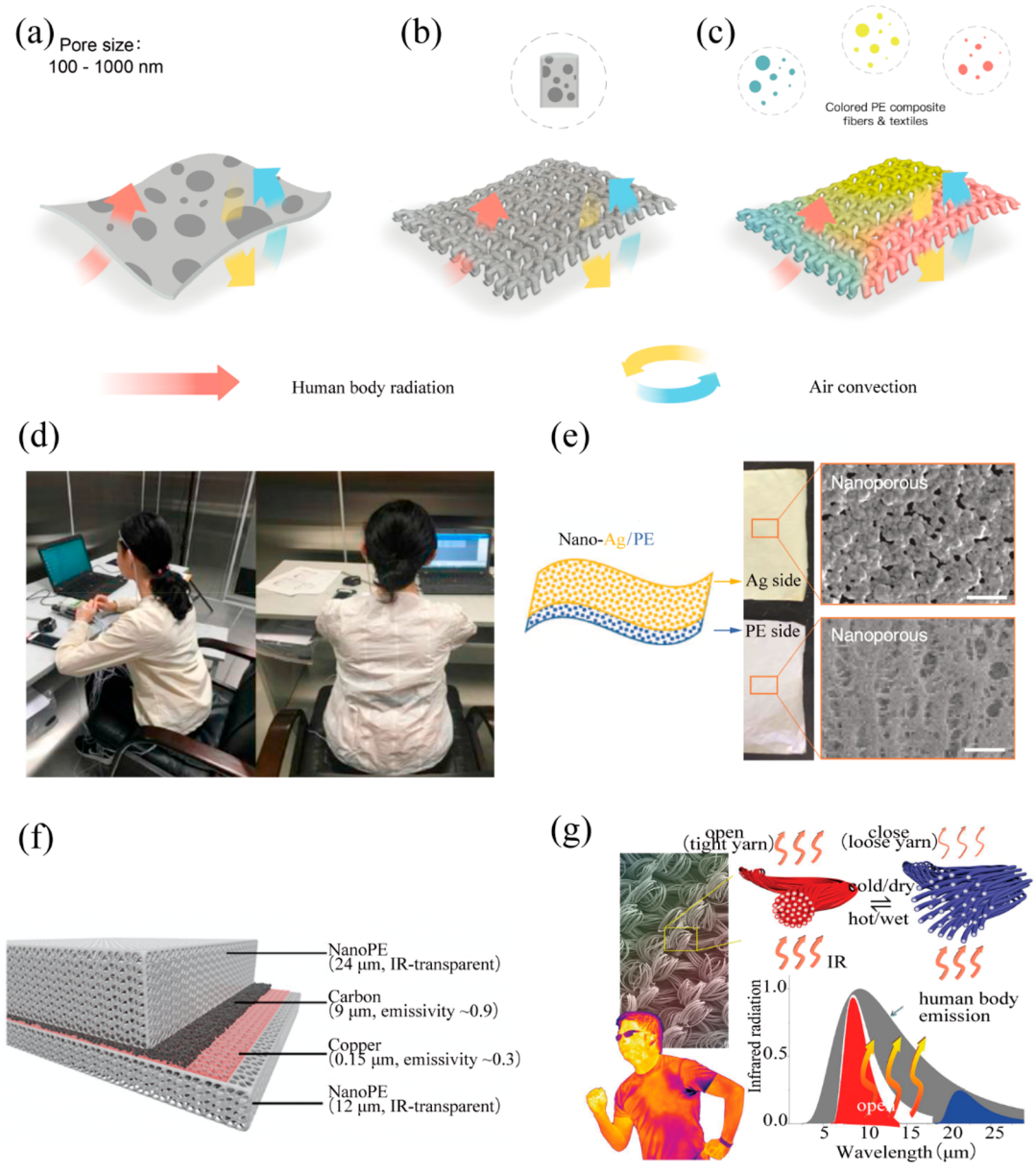

Figure 8. (a) Nanoporous PE film for radiative cooling cloth. (b) The nanoPE fabric for radiative cooling cloth. (c) The nanoPE fabrics with different colors. (d) A female participant wearing the traditional cotton shirt (the left photo) and the nanoPE shirt (the right photo) in testing. Reprinted with permission from ref 93. Copyright 2018 Elsevier. (e) Schematic, photos, and SEM images of nano-Ag/PE material. Reprinted with permission from ref 86. Copyright 2017 Nature Publishing Group. (f) Layered structure of the dual-mode textile. Reprinted with permission from ref 98. Copyright 2017 American Association for the Advancement of Science. (g) The principles of an IR gating textile. Reprinted with permission from ref 100. Copyright 2019 American Association for the Advancement of Science.

environment, textile inner surface, and textile outer surface temperature, respectively.

Tong et al.[85] focused on the influence of mid-IR transmittance and reflectance. The purpose is to have the setpoint temperature as high as possible without compromising personal thermal comfort. Figure 7c shows the maps of the maximum ambient temperature over the cloth's total reflectance and transmittance at different combinations of the air gap thickness t_a and the natural convective heat transfer coefficient h. It can be found that, with the increase of reflectance, the setpoint ambient temperature monotonically decreases independently of t_a and h. For optical properties, it also demonstrated that cooling power increases monotonically with transmittance. This means that materials that are completely transparent in the mid-IR range are the most suitable candidate for cooling. (ii) On the other hand, the heating textile can also be analyzed in a similar way. Unlike the cooling case, the purpose of heating is to decrease the setpoint ambient temperature without making the residents feel cold. Cai et al.[86] analyzed the influence of inner (ε_i) and outer (ε_o) surface emissivity of textiles on the heating effect. The setpoints of ambient temperature for textiles as the function of ε_i and ε_o are shown in Figure 7d. The setpoint decreases monotonically by reducing ε_o at fixed ε_i. However, it remains almost constant when ε_i is changed at fixed ε_o. These results demonstrate the textile's outer surface IR emissivity is the dominant impact on heating performance. Thus, in order to lower the setpoints, the key is to reduce the IR emissivity of the

https://dx.doi.org/10.1021/acsmaterialslett.0c00322
ACS Materials Lett. 2020, 2, 1624−1643

textile's outer surface, which suppresses heat losses from the human body to the ambient environment.

Above all, it is shown that different variables should be considered in cooling and heating cases, even if the thermodynamic model is the same. For cooling, transmittance dominates. On the contrary, the main control knob for heating is emissivity on the textile outer surface.

COOLING

As discussed above, the ideal cooling cloth is IR transparent and can provide passive cooling by the transmission of the human body's thermal radiation directly to the environment. Because of the privacy requirement, it is also expected that the cooling cloth is visibly opaque.[87−93] Tong[85] and Hsu[87] et al. demonstrated this concept based on IR-transparent PE material, which is one of the most common types of IR-transparent cooling materials for personal cooling (see Table 3). Hsu et al.[87] designed the nanoporous PE textile (Figure 8a) that not only possesses air permeability (40−60 $cm^3/s\ cm^2$ Pa), water vapor transmission rate (~0.016 g/cm^2 h), wicking distance (8.3 mm), and mechanical strength (a strip of 2 cm wide nanoPE mesh, which can endure 45 N of tensile force) for wearability but also 77.8% IR transmittance and over 99% visible opacity of optical properties, which resulted in 2.0 °C lower skin temperature than that of the cotton textile.

To demonstrate the scalability and improve the wearability and durability of PE-based cloth, Peng et al.[90] developed a knitted/woven nanoPE microfiber fabric that has cotton-like softness as well as the aforementioned cooling performances (Figure 8b). The knitted/woven fabric has significant improvement of wearability and durability: high water vapor transmission rate of 0.023 g/cm^2 h, wicking rate of 3 cm/30 s, mechanical strength (1.5 cm wide nanoPE fabric can bear a tensile force of about 15 N), and durability (the mid-IR transmittance remains unchanged after five cycles of washing and drying), and it achieved over 80% IR transparency with a fabric thickness of 225 μm. Compared with cotton cloth of the same thickness, the textile composed by nanoPE fibers shows an excellent cooling power, lowering the human skin temperature by 2.3 °C. In order to increase the selection of visible color of the PE cloth to obtain a large wearable market, Cai et al.[91] designed a series of textiles with different color and IR transparent (Figure 8c) by using IR transparency, non-toxic, low-cost pigment nanoparticles, including Prussian blue (PB), iron oxide (Fe_2O_3), and silicon (Si) instead of traditional IR absorbed organic dye molecules with C—O stretching (7.7−10 μm), C—N stretching (8.2−9.8 μm), aromatic C—H bending (7.8−14.5 μm), and S═O stretching (9.4−9.8 μm). After optimization of the concentration and size of inorganic pigment nanoparticles, the result shows that over 80% IR transparency of PE-based cloth with different colors and about 1.6−1.8 °C cooling performance can be obtained with the cotton cloth. In addition, mechanical strength tests show that the maximum tensile force of colored PE composite yarns can reach to ~1.9−2.8 N, which is comparable to the normal cotton yarn. It also shows high stability, with only 3.6% pigment loss after 120 washing cycles. For field testing, Ke et al.[93] demonstrated the actual cooling performance of nanoPE cloth on 18 female participants at four indoor ambient temperatures (23, 25, 27, and 29 °C) (Figure 8d). It has been found that, compared to cotton cloth, the nanoPE cloth obtained lower mean skin temperatures and mean upper torso temperatures at 23, 25, and 27 °C. Meanwhile, they found that most participants feel comfortable at 25 °C when they wear cotton cloth, whereas the temperature is 27 °C for wearing the nanoPE. Thus, the setpoint temperature of air conditioning could be extended from about 25 to 27 °C while wearing nanoPE, which can save about 9−15% energy consumption of the building.[93]

PASSIVE HEATING

For radiative heating, suppression of the human body radiation to the environment is the key, which requires thoughtful designs of high IR reflectance (low emissivity) textiles. Metals such as Ag, Ni, and Cu with high IR reflectance are good candidates. When the breathability of the cloth is taken into account, a metal nanowire network and nano-mesh film were often used[86,94−96] (see Table 3). For example, Cai et al.[86] fabricated a layer of nanoporous Ag film by electroless plating, which serves as an IR reflectance layer added into cloth (Figure 8e). The result shows that, by constructing an IR-reflective layer on an IR-transparent nanoporous layer, heat radiation loss from the human body to the environment can be effectively suppressed without sacrificing wearing comfort: high water vapor transmission rate of 0.012 g/cm^2 h, wicking rate of 1.3 cm/s, ultimate tensile force of 50 N, and laundary durability (the emissivity change is lower than 10% after 10 cycles of washing). Also, the result shows that, compared to normal textile, a 7.1 °C decrease of the setpoint can be achieved, which greatly outperforms other radiative heating textiles (such as Mylar blanket, Omni-Heat) by more than 3 °C. Although a decent heating performance can be achieved so far, we believe the further improvement of wearability and durability of textiles will lead to a more promising future.

COOLING AND PASSIVE HEATING

In real situations, the temperature always changes under spatial and temporal variation of the weather conditions. Traditional methods are either adding/removing the clothing or constantly adjusting the thermostat. However, extra clothing is not always available, and frequent change of thermostat setting is energy-wasting. The ideal solution is to tune the textiles' heat transfer that can dynamically adjust between heating and cooling. So far, Janus cloth, mechanical tuning, and humidity tuning were reported[97−100] (see Table 3). For example, Hsu et al.[98] demonstrate a Janus textile that can perform both passive radiative heating and cooling without extra energy input by adding a bilayer emitter embedded inside an infrared-transparent nanoporous PE layer (Figure 8f). The result shows that the asymmetrical characteristics of both emissivities can achieve two different heat transfer coefficients and heating when the low-emissivity layer is facing outside and cooling when the high-emissivity layer is facing outside. The result shows that the thermal comfort zone of textile can be expanded by 6.5 °C compared with the traditional cloth. Moreover, simulation suggests 14.7 °C of comfort zone expansion for dual-mode textiles with large emissivity contrast. In addition, the air and water vapor permeability of the Janus textile are similar to traditional textiles because the thickness and the morphology of the bilayer emitter are properly engineered. Zhang et al.[100] demonstrated a textile, by coating triacetate−cellulose bimorph fibers with a thin layer of carbon nanotubes (Figure 8g), which achieved more than 35% of infrared radiation tuning as the relative humidity of the underlying skin changed. Both experiments and modeling demonstrate that

https://dx.doi.org/10.1021/acsmaterialslett.0c00322
ACS Materials Lett. 2020, 2, 1624−1643

this dynamic infrared tuning mainly stems from the distance-dependent electromagnetic coupling between neighboring coated fibers in the textile yarns.

OUTLOOK

In the era of climate change and energy crisis, efficient use of energy toward net-zero building is of great importance. Multispectral materials engineering and heat management aim to utilize visible, near-IR, and mid-IR electromagnetic energy for the best of the advantages from a sustainability point of view. The review systematically summarizes the fundamental principles, the state-of-art progress, challenges of sustainable building heat management by daytime radiative cooling, smart windows, and personal thermal management. Some perspectives are listed below:

(1) Radiative cooling: In order to achieve all-year-round energy saving under spatial and temporal variation of the weather conditions, dynamic tuning of heating and cooling of roof technology is highly desirable. Such dynamic tunability will significantly broaden the applicability of this technology and benefit more climate zones. In terms of materials innovations, developing near-perfect selective emitter and mid-IR transparent thermal insulators can bring the cooling performance to the next level.

(2) Smart window: Even though many impressive works were reported on visible tuning and visible/near-IR simultaneous tuning, the independent tuning of visible and near-IR is still rare. With more and more emphasis on the human−building interface aspect of the energy efficiency, we believe the separate control of light and heat could bring immense future opportunities for the science and industry communities.

(3) Personal thermal management: The PE-based passive radiative cooling cloths have somewhat matured and moved toward commercialization. However, the progress on dynamic tuning heating and cooling is still in its preliminary stage. We anticipate dynamic personal thermal management can have profound impacts on not only building energy efficiency but also heat-related personal health. There is still much space for improvement in terms of switching ratio, energy consumption, and incorporation with traditional apparel.

Apart from the technologies mentioned above, solar cells also show attractive prospects in building thermal management. Generally, for household solar panels, >70% of the absorbed solar energy is converted to heat.[101] A photovoltaic thermal system can integrate with a building (façade, roof, windows, etc.) to produce electricity from the solar and thermal energy by utilizing the converted heat of the solar cells, thereby reducing the energy demands of the building. It can also provide daylighting if the semitransparent solar cells were selected, but most are static design.[102] Currently, a dynamic building envelope was developed based on solar cells by the design of a hybrid hard/soft-material actuator, which not only controls the solar gains and daylighting but also generates electricity. For example, in the summer, panels are oriented toward the sun to maximize shading and reduce cooling energy consumption of the building. In winter, open configurations are selected to minimize heating and lighting demands of the building. The result also shows that this dynamic envelope is most effective in temperate and arid climates that can provide up to 115% of the net energy demand of an office room.[103] There are also preliminary works regarding the integration between solar cells and daytime radiative cooling,[104] solar cells, and smart windows.[40,105,106]

AUTHOR INFORMATION

Corresponding Author

Po-Chun Hsu − *Department of Mechanical Engineering and Materials Science, Duke University, Durham, North Carolina 27708, United States;* orcid.org/0000-0002-6509-9377; Email: pochun.hsu@duke.edu

Authors

Xiuqiang Li − *Department of Mechanical Engineering and Materials Science, Duke University, Durham, North Carolina 27708, United States*

Wanrong Xie − *Department of Mechanical Engineering and Materials Science, Duke University, Durham, North Carolina 27708, United States*

Chenxi Sui − *Department of Mechanical Engineering and Materials Science, Duke University, Durham, North Carolina 27708, United States*

Complete contact information is available at: https://pubs.acs.org/10.1021/acsmaterialslett.0c00322

Notes

The authors declare no competing financial interest.

ACKNOWLEDGMENTS

We thank Pratt School of Engineering at Duke University for the funding support.

REFERENCES

(1) Heating & Cooling | Department of Energy; www.energy.gov/heating-cooling.

(2) Ürge-Vorsatz, D.; et al. In *Climate Change* 2014: *Mitigation* (Intergovernmental Panel on Climate Change, 2014), Chapter 9: Buildings.

(3) Raman, A. P.; Anoma, M. A.; Zhu, L.; Rephaeli, E.; Fan, S. Passive radiative cooling below ambient air temperature under direct sunlight. *Nature* **2014**, *515*, 540−544.

(4) Zhao, D.; Aili, A.; Zhai, Y.; Xu, S.; Tan, G.; Yin, X.; Yang, R. Radiative sky cooling: fundamental principles, materials, and applications. *Appl. Phys. Rev.* **2019**, *6*, 021306.

(5) Goldstein, E. A.; Raman, A. P.; Fan, S. Sub-ambient non-evaporative fluid cooling with the sky. *Nature Energy* **2017**, *2*, 17143.

(6) Ke, Y.; Chen, J.; Lin, G.; Wang, S.; Zhou, Y.; Yin, J.; Lee, P. S.; Long, Y. Smart windows: electro-, thermo-, mechano-, photochromics, and beyond. *Adv. Energy Mater.* **2019**, *9*, 1902066.

(7) Peng, L.; Su, B.; Yu, A.; Jiang, X. Review of clothing for thermal management with advanced materials. *Cellulose* **2019**, *26*, 6415−6448.

(8) Zhao, D.; Lu, X.; Fan, T.; Wu, Y. S.; Lou, L.; Wang, Q.; Fan, J.; Yang, R. Personal thermal management using portable thermoelectrics for potential building energy saving. *Appl. Energy* **2018**, *218*, 282−291.

(9) Harrison, A. Radiative cooling of TiO_2 white panint. *Sol. Energy* **1978**, *20*, 185−188.

(10) Bhatia, B.; Leroy, A.; Shen, Y.; Zhao, L.; Gianello, M.; Li, D.; Gu, T.; Hu, J.; Soljacic, M.; Wang, E. N. Passive directional sub-ambient daytime radiative cooling. *Nat. Commun.* **2018**, *9*, 5001.

(11) Chen, Z.; Zhu, L.; Li, W.; Fan, S. Simultaneously and synergistically harvest energy from the sun and outer space. *Joule* **2019**, *3*, 101−110.

(12) Chen, Z.; Zhu, L.; Raman, A.; Fan, S. Radiative cooling to deep sub-freezing temperatures through a 24-h day-night cycle. *Nat. Commun.* **2016**, *7*, 13729.
(13) Fang, H.; Zhao, D.; Yuan, J.; Aili, A.; Yin, X.; Yang, R.; Tan, G. Performance evaluation of a metamaterial-based new cool roof using improved roof thermal transfer value model. *Appl. Energy* **2019**, *248*, 589−599.
(14) Kou, J.; Jurado, Z.; Chen, Z.; Fan, S.; Minnich, A. J. Daytime radiative cooling using near-black infrared emitters. *ACS Photonics* **2017**, *4*, 626−30.
(15) Gentle, A. R.; Smith, G. B. A Subambient open roof surface under the mid-summer sun. *Advanced Science (Weinh)* **2015**, *2*, 1500119.
(16) Ko, B.; Lee, D.; Badloe, T.; Rho, J. Metamaterial-based radiative cooling: towards energy-free all-day cooling. *Energies* **2019**, *12*, 89.
(17) Leroy, A.; Bhatia, B.; Kelsall, C. C.; Castillejo-Cuberos, A.; Di Capua, H. M.; Zhao, L.; Zhang, L.; Guzman, A. M.; Wang, E. N. High-performance subambient radiative cooling enabled by optically selective and thermally insulating polyethylene aerogel. *Science Advances* **2019**, *5*, eaat9480.
(18) Li, T.; Zhai, Y.; He, S.; Gan, W.; Wei, Z.; Heidarinejad, M.; Dalgo, D.; Mi, R.; Zhao, X.; Song, J.; Dai, J.; Chen, C.; Aili, A.; Vellore, A.; Martini, A.; Yang, R.; Srebric, J.; Yin, X.; Hu, L. A radiative cooling structural material. *Science* **2019**, *364*, 760−763.
(19) Li, W.; Shi, Y.; Chen, Z.; Fan, S. Photonic thermal management of coloured objects. *Nat. Commun.* **2018**, *9*, 4240.
(20) Mandal, J.; Fu, Y.; Overvig, A. C.; Jia, M.; Sun, K.; Shi, N. N.; Zhou, H.; Xiao, X.; Yu, N.; Yang, Y. Hierarchically porous polymer coatings for highly efficient passive daytime radiative cooling. *Science* **2018**, *362*, 315−319.
(21) Raman, A. P.; Li, W.; Fan, S. Generating light from darkness. *Joule* **2019**, *3*, 2679−2686.
(22) Wang, W.; Fernandez, N.; Katipamula, S.; Alvine, K. Performance assessment of a photonic radiative cooling system for office buildings. *Renewable Energy* **2018**, *118*, 265−277.
(23) Zhai, Y.; Ma, Y.; David, S. N.; Zhao, D.; Lou, R.; Tan, G.; Yang, R.; Yin, X. Scalable-manufactured randomized glass-polymer hybrid metamaterial for daytime radiative cooling. *Science* **2017**, *355*, 1062−1066.
(24) Zhang, K.; Zhao, D.; Yin, X.; Yang, R.; Tan, G. Energy saving and economic analysis of a new hybrid radiative cooling system for single-family houses in the USA. *Appl. Energy* **2018**, *224*, 371−381.
(25) Zhao, D.; Aili, A.; Yin, X.; Tan, G.; Yang, R. Roof-integrated radiative air-cooling system to achieve cooler attic for building energy saving. *Energy and Buildings* **2019**, *203*, 109453.
(26) Zhao, D.; Aili, A.; Zhai, Y.; Lu, J.; Kidd, D.; Tan, G.; Yin, X.; Yang, R. Subambient cooling of water: toward real-world applications of daytime radiative cooling. *Joule* **2019**, *3*, 111−123.
(27) Zhou, L.; Song, H.; Liang, J.; Singer, M.; Zhou, M.; Stegenburgs, E.; Zhang, N.; Xu, C.; Ng, T.; Yu, Z.; Ooi, B.; Gan, Q. A polydimethylsiloxane-coated metal structure for all-day radiative cooling. *Nature Sustainability* **2019**, *2*, 718−724.
(28) Zhu, L.; Raman, A. P.; Fan, S. Radiative cooling of solar absorbers using a visibly transparent photonic crystal thermal blackbody. *Proc. Natl. Acad. Sci. U. S. A.* **2015**, *112*, 12282−12287.
(29) https://ntrs.nasa.gov/search.jsp?R=19930010877.
(30) Eriksson, T.; Granqvist, C. Radiative cooling computed for model atmospheres. *Appl. Opt.* **1982**, *21*, 4381−4388.
(31) Khandelwal, H.; Schenning, A. P. H. J.; Debije, M. G. Infrared regulating smart window based on organic materials. *Advanced Energy Materials* **2017**, *7*, 1602209.
(32) Kim, H. N.; Yang, S. Responsive smart windows from nanoparticle−polymer composites. *Adv. Funct. Mater.* **2020**, *30*, 1902597.
(33) Cai, G.; Cui, M.; Kumar, V.; Darmawan, P.; Wang, J.; Wang, X.; Lee-Sie Eh, A.; Qian, K.; Lee, P. S. Ultra-large optical modulation of electrochromic porous WO3 film and the local monitoring of redox activity. *Chemical Science* **2016**, *7*, 1373−1382.
(34) Cheng, W.; He, J.; Dettelbach, K. E.; Johnson, N. J. J.; Sherbo, R. S.; Berlinguette, C. P. Photodeposited amorphous oxide films for electrochromic windows. *Chem* **2018**, *4*, 821−832.
(35) Davy, N. C.; Sezen-Edmonds, M.; Gao, J.; Lin, X.; Liu, A.; Yao, N.; Kahn, A.; Loo, Y.-L. Pairing of near-ultraviolet solar cells with electrochromic windows for smart management of the solar spectrum. *Nature Energy* **2017**, *2*, 17104.
(36) Hsu, C. Y.; Zhang, J.; Sato, T.; Moriyama, S.; Higuchi, M. Black-to-transmissive electrochromism with visible-to-near-infrared switching of a Co(II)-based metallo-supramolecular polymer for smart window and digital signage applications. *ACS Appl. Mater. Interfaces* **2015**, *7*, 18266−72.
(37) Khandelwal, H.; Loonen, R. C.; Hensen, J. L.; Debije, M. G.; Schenning, A. P. Electrically switchable polymer stabilised broadband infrared reflectors and their potential as smart windows for energy saving in buildings. *Sci. Rep.* **2015**, *5*, 11773.
(38) Kiruthika, S.; Kulkarni, G. U. Energy efficient hydrogel based smart windows with low cost transparent conducting electrodes. *Sol. Energy Mater. Sol. Cells* **2017**, *163*, 231−236.
(39) Shin, H.; Seo, S.; Park, C.; Na, J.; Han, M.; Kim, E. Energy saving electrochromic windows from bistable low-HOMO level conjugated polymers. *Energy Environ. Sci.* **2016**, *9*, 117−122.
(40) Xia, X.; Ku, Z.; Zhou, D.; Zhong, Y.; Zhang, Y.; Wang, Y.; Huang, M. J.; Tu, J.; Fan, H. J. Perovskite solar cell powered electrochromic batteries for smart windows. *Mater. Horiz.* **2016**, *3*, 588−595.
(41) Xu, J.; Zhang, Y.; Zhai, T. T.; Kuang, Z.; Li, J.; Wang, Y.; Gao, Z.; Song, Y. Y.; Xia, X. H. Electrochromic-tuned plasmonics for photothermal sterile window. *ACS Nano* **2018**, *12*, 6895−6903.
(42) Nguyen, T. D.; Yeo, L. P.; Kei, T. C.; Mandler, D.; Magdassi, S.; Tok, A. I. Y. Efficient near infrared modulation with high visible transparency using SnO_2 −WO_3 nanostructure for advanced smart windows. *Adv. Opt. Mater.* **2019**, *7*, 1801389.
(43) Llordés, A; Garcia, G; Gazquez, J; et al. Tunable near-infrared and visible-light transmittance in nanocrystal-in-glass composites. *Nature* **2013**, *500*, 323−326.
(44) Barile, C. J.; Slotcavage, D. J.; McGehee, M. D. Polymer−nanoparticle electrochromic materials that selectively modulate visible and near-infrared light. *Chem. Mater.* **2016**, *28*, 1439−1445.
(45) Cao, S.; Zhang, S.; Zhang, T.; Yao, Q.; Lee, J. Y. A visible light-near-infrared dual-band smart window with internal energy storage. *Joule* **2019**, *3*, 1152−1162.
(46) Hernandez, T. S.; Barile, C. J.; Strand, M. T.; Dayrit, T. E.; Slotcavage, D. J.; McGehee, M. D. Bistable black electrochromic windows based on the reversible metal electrodeposition of Bi and Cu. *ACS Energy Letters* **2018**, *3*, 104−111.
(47) Islam, S. M.; Hernandez, T. S.; McGehee, M. D.; Barile, C. J. Hybrid dynamic windows using reversible metal electrodeposition and ion insertion. *Nature Energy* **2019**, *4*, 223−229.
(48) Rai, V.; Tiwari, N.; Rajput, M.; Joshi, S. M.; Nguyen, A. C.; Mathews, N. Reversible electrochemical silver deposition over large areas for smart windows and information display. *Electrochim. Acta* **2017**, *255*, 63−71.
(49) Chen, C.-W.; Brigeman, A. N.; Ho, T.-J.; Khoo, I. C. Normally transparent smart window based on electrically induced instability in dielectrically negative cholesteric liquid crystal. *Opt. Mater. Express* **2018**, *8*, 691−697.
(50) Sun, H.; Xie, Z.; Ju, C.; Hu, X.; Yuan, D.; Zhao, W.; Shui, L.; Zhou, G. Dye-doped electrically smart windows based on polymer-stabilized liquid crystal. *Polymers (Basel, Switz.)* **2019**, *11*, 694.
(51) Sol, J. A. H. P.; Timmermans, G. H.; van Breugel, A. J.; Schenning, A. P. H. J.; Debije, M. G. Multistate luminescent solar concentrator "smart" windows. *Advanced Energy Materials* **2018**, *8*, 1702922.
(52) Hosseinzadeh Khaligh, H.; Liew, K.; Han, Y.; Abukhdeir, N. M.; Goldthorpe, I. A. Silver nanowire transparent electrodes for liquid crystal-based smart windows. *Sol. Energy Mater. Sol. Cells* **2015**, *132*, 337−341.

https://dx.doi.org/10.1021/acsmaterialslett.0c00322
ACS Materials Lett. 2020, 2, 1624−1643

(53) Ke, Y.; Zhou, C.; Zhou, Y.; Wang, S.; Chan, S. H.; Long, Y. Emerging thermal-responsive materials and integrated techniques targeting the energy-efficient smart window application. *Adv. Funct. Mater.* **2018**, *28*, 1800113.
(54) Zhu, J.; Huang, A.; Ma, H.; Ma, Y.; Tong, K.; Ji, S.; Bao, S.; Cao, X.; Jin, P. Composite film of vanadium dioxide nanoparticles and ionic liquid-nickel-chlorine complexes with excellent visible thermochromic performance. *ACS Appl. Mater. Interfaces* **2016**, *8*, 29742−29748.
(55) Chen, Y.; Zhu, J.; Ma, H.; Chen, L.; Li, R.; Jin, P. VO2/Nickel-bromine-ionic liquid composite film for thermochromic application. *Sol. Energy Mater. Sol. Cells* **2019**, *196*, 124−130.
(56) De Bastiani, M.; Saidaminov, M. I.; Dursun, I.; Sinatra, L.; Peng, W.; Buttner, U.; Mohammed, O. F.; Bakr, O. M. Thermochromic perovskite inks for reversible smart window applications. *Chem. Mater.* **2017**, *29*, 3367−3370.
(57) Ke, Y.; Balin, I.; Wang, N.; Lu, Q.; Tok, A. I.; White, T. J.; Magdassi, S.; Abdulhalim, I.; Long, Y. Two-dimensional SiO_2/VO_2 photonic crystals with statically visible and dynamically infrared modulated for smart window deployment. *ACS Appl. Mater. Interfaces* **2016**, *8*, 33112−33120.
(58) Cui, Y.; Ke, Y.; Liu, C.; Chen, Z.; Wang, N.; Zhang, L.; Zhou, Y.; Wang, S.; Gao, Y.; Long, Y. Thermochromic VO2 for energy-efficient smart windows. *Joule* **2018**, *2*, 1707−1746.
(59) Hao, Q.; Li, W.; Xu, H.; Wang, J.; Yin, Y.; Wang, H.; Ma, L.; Ma, F.; Jiang, X.; Schmidt, O. G.; Chu, P. K. VO2 /TiN plasmonic thermochromic smart coatings for room-temperature applications. *Adv. Mater.* **2018**, *30*, 1705421.
(60) Vu, T. D.; Chen, Z.; Zeng, X.; Jiang, M.; Liu, S.; Gao, Y.; Long, Y. Physical vapour deposition of vanadium dioxide for thermochromic smart window applications. *J. Mater. Chem. C* **2019**, *7*, 2121−2145.
(61) Liang, X.; Guo, C.; Chen, M.; Guo, S.; Zhang, L.; Li, F.; Guo, S.; Yang, H. A roll-to-roll process for multi-responsive soft-matter composite films containing Cs_xWO_3 nanorods for energy-efficient smart window applications. *Nanoscale Horizons* **2017**, *2*, 319−325.
(62) Li, X.-H.; Liu, C.; Feng, S.-P.; Fang, N. X. Broadband light management with thermochromic hydrogel microparticles for smart windows. *Joule* **2019**, *3*, 290−302.
(63) Ge, D.; Lee, E.; Yang, L.; Cho, Y.; Li, M.; Gianola, D. S.; Yang, S. A robust smart window: reversibly switching from high transparency to angle-independent structural color display. *Adv. Mater.* **2015**, *27*, 2489−2495.
(64) Kim, H. N.; Ge, D.; Lee, E.; Yang, S. Multistate and on-demand smart windows. *Adv. Mater.* **2018**, *30*, 1803847.
(65) Lin, G.; Chandrasekaran, P.; Lv, C.; Zhang, Q.; Tang, Y.; Han, L.; Yin, J. Self-similar hierarchical wrinkles as a potential multifunctional smart window with simultaneously tunable transparency, structural color, and droplet transport. *ACS Appl. Mater. Interfaces* **2017**, *9*, 26510−26517.
(66) Shrestha, M.; Asundi, A.; Lau, G.-K. Smart window based on electric unfolding of microwrinkled TiO2 nanometric films. *ACS Photonics* **2018**, *5*, 3255−3262.
(67) Tang, Y.; Lin, G.; Yang, S.; Yi, Y. K.; Kamien, R. D.; Yin, J. Programmable kiri-kirigami metamaterials. *Adv. Mater.* **2017**, *29*, 1604262.
(68) Zhang, Y.; Yan, Z.; Nan, K.; Xiao, D.; Liu, Y.; Luan, H.; Fu, H.; Wang, X.; Yang, Q.; Wang, J.; Ren, W.; Si, H.; Liu, F.; Yang, L.; Li, H.; Wang, J.; Guo, X.; Luo, H.; Wang, L.; Huang, Y.; Rogers, J. A. A mechanically driven form of Kirigami as a route to 3D mesostructures in micro/nanomembranes. *Proc. Natl. Acad. Sci. U. S. A.* **2015**, *112*, 11757−11764.
(69) Ke, Y.; Yin, Y.; Zhang, Q.; Tan, Y.; Hu, P.; Wang, S.; Tang, Y.; Zhou, Y.; Wen, X.; Wu, S.; White, T. J.; Yin, J.; Peng, J.; Xiong, Q.; Zhao, D.; Long, Y. Adaptive thermochromic windows from active plasmonic elastomers. *Joule* **2019**, *3*, 858−871.
(70) Mandal, J.; Jia, M.; Overvig, A.; Fu, Y.; Che, E.; Yu, N.; Yang, Y. Porous polymers with switchable optical transmittance for optical and thermal regulation. *Joule* **2019**, *3*, 3088−3099.
(71) Adachi, K.; Tokushige, M.; Omata, K.; Yamazaki, S.; Iwadate, Y. Kinetics of coloration in photochromic tungsten(VI) oxide/silicon oxycarbide/silica hybrid xerogel: insight into cation self-diffusion mechanisms. *ACS Appl. Mater. Interfaces* **2016**, *8*, 14019−14028.
(72) Bella, F.; Leftheriotis, G.; Griffini, G.; Syrrokostas, G.; Turri, S.; Grätzel, M.; Gerbaldi, C. A new design paradigm for smart windows: photocurable polymers for quasi-solid photoelectrochromic devices with excellent long-term stability under real outdoor operating conditions. *Adv. Funct. Mater.* **2016**, *26*, 1127−1137.
(73) Kuroiwa, H.; Inagaki, Y.; Mutoh, K.; Abe, J. On-demand control of the photochromic properties of naphthopyrans. *Adv. Mater.* **2019**, *31*, 1805661.
(74) Yu, Z.; Yao, Y.; Yao, J.; Zhang, L.; Chen, Z.; Gao, Y.; Luo, H. Transparent wood containing CsxWO3 nanoparticles for heat-shielding window applications. *J. Mater. Chem. A* **2017**, *5*, 6019−6024.
(75) Lee, S. J.; Choi, D. S.; Kang, S. H.; Yang, W. S.; Nahm, S.; Han, S. H.; Kim, T. VO_2/WO_3-based hybrid smart windows with thermochromic and electrochromic properties. *ACS Sustainable Chem. Eng.* **2019**, *7*, 7111−7117.
(76) Peng, Y; Cui, Y. Advanced textiles for personal thermal management and energy. *Joule* **2020**, *4*, 724−742.
(77) Cui, Y.; Gong, H.; Wang, Y.; Li, D.; Bai, H. A thermally insulating textile inspired by polar bear hair. *Adv. Mater.* **2018**, *30*, 1706807.
(78) Dai, B.; Li, K.; Shi, L.; Wan, X.; Liu, X.; Zhang, F.; Jiang, L.; Wang, S. Bioinspired janus textile with conical micropores for human body moisture and thermal management. *Adv. Mater.* **2019**, *31*, 1904113.
(79) Gao, T.; Yang, Z.; Chen, C.; Li, Y.; Fu, K.; Dai, J.; Hitz, E. M.; Xie, H.; Liu, B.; Song, J.; Yang, B.; Hu, L. Three-dimensional printed thermal regulation textiles. *ACS Nano* **2017**, *11*, 11513−11520.
(80) Hong, S.; Gu, Y.; Seo, J. K.; Wang, J.; Liu, P.; Meng, Y. S.; Xu, S.; Chen, R. J. S. a. Wearable thermoelectrics for personalized thermoregulation. *Science advances* **2019**, *5*, eaaw0536.
(81) Liu, Z.; Lyu, J.; Fang, D.; Zhang, X. Nanofibrous kevlar aerogel threads for thermal insulation in harsh environments. *ACS Nano* **2019**, *13*, 5703−5711.
(82) Wang, Y.; Liang, X.; Zhu, H.; Xin, J. H.; Zhang, Q.; Zhu, S. Reversible water transportation diode: temperature-adaptive smart janus textile for moisture/thermal management. *Adv. Funct. Mater.* **2020**, *30*, 1907851.
(83) Guo, Y.; Dun, C.; Xu, J.; Mu, J.; Li, P.; Gu, L.; Hou, C.; Hewitt, C. A.; Zhang, Q.; Li, Y.; Carroll, D. L.; Wang, H. Ultrathin, washable, and large-area graphene papers for personal thermal management. *Small* **2017**, *13*, 1702645.
(84) Guo, Y.; Li, K.; Hou, C.; Li, Y.; Zhang, Q.; Wang, H. Fluoroalkylsilane-modified textile-based personal energy management device for multifunctional wearable applications. *ACS Appl. Mater. Interfaces* **2016**, *8*, 4676−4683.
(85) Tong, J. K.; Huang, X.; Boriskina, S. V.; Loomis, J.; Xu, Y.; Chen, G. Infrared-transparent visible-opaque fabrics for wearable personal thermal management. *ACS Photonics* **2015**, *2*, 769−778.
(86) Cai, L.; Song, A. Y.; Wu, P.; Hsu, P. C.; Peng, Y.; Chen, J.; Liu, C.; Catrysse, P. B.; Liu, Y.; Yang, A.; Zhou, C.; Zhou, C.; Fan, S.; Cui, Y. Warming up human body by nanoporous metallized polyethylene textile. *Nat. Commun.* **2017**, *8*, 496.
(87) Hsu, P.-C.; Song, A. Y.; Catrysse, P. B.; Liu, C.; Peng, Y.; Xie, J.; Fan, S.; Cui, Y. Radiative human body cooling by nanoporous polyethylene textile. *Science* **2016**, *353*, 1019−1023.
(88) Catrysse, P. B.; Song, A. Y.; Fan, S. Photonic structure textile design for localized thermal cooling based on a fiber blending scheme. *ACS Photonics* **2016**, *3*, 2420−2426.
(89) Lozano, L. M.; Hong, S.; Huang, Y.; Zandavi, H.; El Aoud, Y. A.; Tsurimaki, Y.; Zhou, J.; Xu, Y.; Osgood, R. M.; Chen, G.; Boriskina, S. V. Optical engineering of polymer materials and composites for simultaneous color and thermal management. *Opt. Mater. Express* **2019**, *9*, 1990−2005.
(90) Peng, Y.; Chen, J.; Song, A. Y.; Catrysse, P. B.; Hsu, P.-C.; Cai, L.; Liu, B.; Zhu, Y.; Zhou, G.; Wu, D. S.; Lee, H. R.; Fan, S.; Cui, Y.

https://dx.doi.org/10.1021/acsmaterialslett.0c00322
ACS Materials Lett. 2020, 2, 1624−1643

Nanoporous polyethylene microfibres for large-scale radiative cooling fabric. *Nature Sustainability* **2018**, *1*, 105−112.
(91) Cai, L.; Peng, Y.; Xu, J.; Zhou, C.; Zhou, C.; Wu, P.; Lin, D.; Fan, S.; Cui, Y. Temperature regulation in colored infrared-transparent polyethylene textiles. *Joule* **2019**, *3*, 1478−1486.
(92) Yang, A.; Cai, L.; Zhang, R.; Wang, J.; Hsu, P. C.; Wang, H.; Zhou, G.; Xu, J.; Cui, Y. Thermal management in nanofiber-based face mask. *Nano Lett.* **2017**, *17*, 3506−3510.
(93) Ke, Y.; Wang, F.; Xu, P.; Yang, B. On the use of a novel nanoporous polyethylene (nanoPE) passive cooling material for personal thermal comfort management under uniform indoor environments. *Building and Environment* **2018**, *145*, 85−95.
(94) Hazarika, A.; Deka, B. K.; Kim, D.; Jeong, H. E.; Park, Y. B.; Park, H. W. Woven kevlar fiber/polydimethylsiloxane/reduced graphene oxide composite-based personal thermal management with freestanding Cu-Ni core-shell nanowires. *Nano Lett.* **2018**, *18*, 6731−6739.
(95) Hsu, P. C.; Liu, X.; Liu, C.; Xie, X.; Lee, H. R.; Welch, A. J.; Zhao, T.; Cui, Y. Personal thermal management by metallic nanowire-coated textile. *Nano Lett.* **2015**, *15*, 365−71.
(96) Liu, Q.; Huang, J.; Zhang, J.; Hong, Y.; Wan, Y.; Wang, Q.; Gong, M.; Wu, Z.; Guo, C. F. Thermal, waterproof, breathable, and antibacterial cloth with a nanoporous structure. *ACS Appl. Mater. Interfaces* **2018**, *10*, 2026−2032.
(97) Yue, X.; Zhang, T.; Yang, D.; Qiu, F.; Wei, G.; Zhou, H. Multifunctional janus fibrous hybrid membranes with sandwich structure for on-demand personal thermal management. *Nano Energy* **2019**, *63*, 103808.
(98) Hsu, P. C.; Liu, C.; Song, A. Y.; Zhang, Z.; Peng, Y.; Xie, J.; Liu, K.; Wu, C. L.; Catrysse, P. B.; Cai, L.; Zhai, S.; Majumdar, A.; Fan, S.; Cui, Y. A dual-mode textile for human body radiative heating and cooling. *Science Advances* **2017**, *3*, e1700895.
(99) Leung, E. M.; Colorado Escobar, M.; Stiubianu, G. T.; Jim, S. R.; Vyatskikh, A. L.; Feng, Z.; Garner, N.; Patel, P.; Naughton, K. L.; Follador, M.; Karshalev, E.; Trexler, M. D.; Gorodetsky, A. A. A dynamic thermoregulatory material inspired by squid skin. *Nat. Commun.* **2019**, *10*, 1947.
(100) Zhang, X. A.; Yu, S.; Xu, B.; Li, M.; Peng, Z.; Wang, Y.; Deng, S.; Wu, X.; Wu, Z.; Ouyang, M.; Wang, Y. Dynamic gating of infrared radiation in a textile. *Science* **2019**, *363*, 619−623.
(101) Xu, N.; Zhu, P.; Sheng, Y.; Zhou, L.; Li, X.; Tan, H.; Zhu, J. Synergistic tandem solar electricity-water generators. *Joule* **2020**, *4*, 347−358.
(102) Gupta, N.; Tiwari, G. N. Review of passive heating/cooling systems of buildings. *Energy Sci. Eng.* **2016**, *4*, 305−333.
(103) Svetozarevic, B.; Begle, M.; Jayathissa, P.; Caranovic, S.; Shepherd, R. F.; Nagy, Z.; Schlueter, A. Dynamic photovoltaic building envelopes for adaptive energy and comfort management. *Nature Energy* **2019**, *4*, 671−682.
(104) Chen, Z.; Zhu, L.; Li, W.; Fan, S. Simultaneously and synergistically harvest energy from the sun and outer space. *Joule* **2019**, *3*, 101−110.
(105) Lin, J.; Lai, M.; Dou, L.; Kley, C. S.; Chen, H.; Peng, F.; et al. Thermochromic halide perovskite solar cells. *Nat. Mater.* **2018**, *17*, 261−267.
(106) Davy, N. C.; Sezen-Edmonds, M.; Gao, J.; Lin, X.; Liu, A.; Yao, N.; Kahn, A.; Loo, Y. L. Pairing of near-ultraviolet solar cells with electrochromic windows for smart management of the solar spectrum. *Nature Energy* **2017**, *2*, 17104.

https://dx.doi.org/10.1021/acsmaterialslett.0c00322
ACS Materials Lett. 2020, 2, 1624−1643